



Andaman–Nicobar–Sumatra Margin Revisited: Analysis of the Lithospheric Structure and Deformation Based on Gravity Modeling and Distribution of Seismicity

Sk. Shamim¹ · Prosanta Kumar Khan¹ · Sarada P. Mohanty² · Manoranjan Mohanty³

Received: 12 October 2019 / Accepted: 27 January 2021 / Published online: 14 February 2021
© The Author(s), under exclusive licence to Springer Nature B.V. part of Springer Nature 2021

Abstract

The Andaman–Nicobar–Sumatra subduction margin, with a well-developed Benioff zone down to ~200 km depth, extends over 1300 km along strike and has a lateral extent of ~200 km. Two-dimensional (2D) profiles based on generalized inversion of free-air gravity anomaly data across different segments of the Andaman–Nicobar sector of the margin were analyzed by reconstructing the geometry of the converging India–Eurasia lithospheric plates. Detailed 2D structures of the Ninetyeast Ridge (NER), fore-arc basin, volcanic arc, back-arc basin, spreading ridge, Sewell Rise, Mergui Ridge and Mergui Basin, and depths of Moho and the lithosphere–asthenosphere boundary were delineated. The volcanic arc is located at a distance of ~150–200 km from the trench and is marked by a zone of positive gravity anomaly separated from the trench by the fore-arc basin with a zone of gravity low. The topographic and gravity anomaly patterns show complex geometrical patterns over the volcanic arc due to the presence of a number of regional faults striking parallel to the trench axis developing a series of pull-apart (transtensional) basins as well as the interaction of the spreading ridges on the overriding plate. A narrow zone of negative gravity anomaly (~–185 to –110 mGal) observed in the gravity model of the margin is interpreted to be associated with fore-arc shear fault above a zone of fractured oceanic crust with a thick sedimentary layer, located above a zone of sharp bending of the eastward converging Indian lithosphere in the fore-arc basin. A high concentration of seismicity and a trench-parallel band of moderate moment energy release along this fault might have been caused by concentrated deformation within the zone of flexing of the descending plate. A wide fore-arc (>200 km) and the enhanced deformation of the subducting Indian oceanic plate in central sectors possibly resulted from increased interaction between the NER and the Andaman trench and extension in the Andaman back-arc. Appearance of a second moderate energy band and shifting of seismicity toward the trench axis following the 2004 M_W 9.2 mega-event are apparently caused by the migration of the stress field from deeper to shallower part of the Indian lithosphere. A similar type of seismicity migration toward shallower part of the descending plate has been recorded along other subduction margins around the globe.

Keywords Convergent margin seismicity · 2D gravity modeling · Andaman–Nicobar–Sumatra margin · Lithosphere · Deformation

Article Highlights

- Deformation of lithosphere along the oblique Andaman–Nicobar–Sumatra subduction margin,
- Inversion and modeling of the lithosphere using free-air gravity anomaly and topography data
- Seismic activities and energy release characteristics during the 2004 mega-earthquake ($M_w > 9.0$)

1 Introduction

Deformation of the lithosphere along a subduction zone is primarily manifested by the stress release (~90%) in the form of earthquakes, and the remaining stress contributes toward the bending of the plate (Turcotte and Schubert 1982). It was observed that the flexing zones of the descending lithosphere are the nodal areas of stress concentration, which release most of the strain energy during a great earthquake along the subduction margins (Conrad and Hager 1999; Khan and Chakraborty 2009). Our analyses make an attempt to understand the genetic linkage between different tectonic elements and occurrences of earthquakes under the pre- and post-seismic phases of the 2004 M_w 9.2 off-Sumatra mega-event.

The complex and unique tectonic setup of the ~1300-km-long Andaman–Sumatra subduction margin (Fig. 1) is characterized by oblique convergence of the Indian oceanic lithosphere against the Eurasian plate, variable subduction rate along the trench, development of several fault systems with concomitant rotation of microplates in the overriding zone and presence of regional transtension regime with poorly defined spreading centers (Fitch 1972; Mitchell 1981; McCaffrey 1992; Dasgupta et al. 2003; Kamesh Raju et al. 2004; Curray 2005; Khan and Chakraborty 2005; Chakraborty and Khan 2009; Morley and Searle 2017). The velocity as well as the convergence of the Indo-Australian plate against the Eurasian plate had significant variations from north to northeast during the Cenozoic (DeMets et al. 1994). The complex tectonics of the provinces resulted in the development of different marginal basins (e.g., Andaman Sea, Mergui Basin, Sumatra Basin) on the overriding plate, and variable decoupling of the microplates from the overriding Eurasian plate along the trench axis (Curray et al. 1979; Tapponnier et al. 1986; Maung 1987; Hall 1996; McCaffrey et al. 2000; Kamesh Raju et al. 2004; Chakraborty and Khan 2009).

Seismicity across the Andaman–Nicobar–Sumatra boundary depends on several factors: (a) plate obliquity (Khan and Chakraborty 2005), (b) stress obliquity (Khan 2007), (c) subduction rate (Cao and Gao 2002), (d) structural heterogeneities (Cloos 1992; Prawirodirdjo et al. 2010; Henstock et al. 2017; Shamim et al. 2019), (e) degree of seismic coupling, (f) co- and post-seismic slip history (Subarya et al. 2006; Chlieh et al. 2007; Bletery et al. 2016), (g) co- and post-seismic moment energy release (Ishii et al. 2005; Lay et al. 2005; Chlieh et al. 2007), (h) stress perturbation (Khan et al. 2020), and (i) the overall geometry of the underriding plate (Khan et al. 2017, 2018). These properties can change the level of seismicity at any arbitrary location both in the underriding and overriding plate. Although the degree of seismic coupling can explain the occurrences of small-to-moderate scale seismicity, it fails to account for the locale of great shallow earthquakes ($M_w \geq 8.5$) along the Java-Bengal sector (Conrad et al. 2004). The historical records of ~200 years

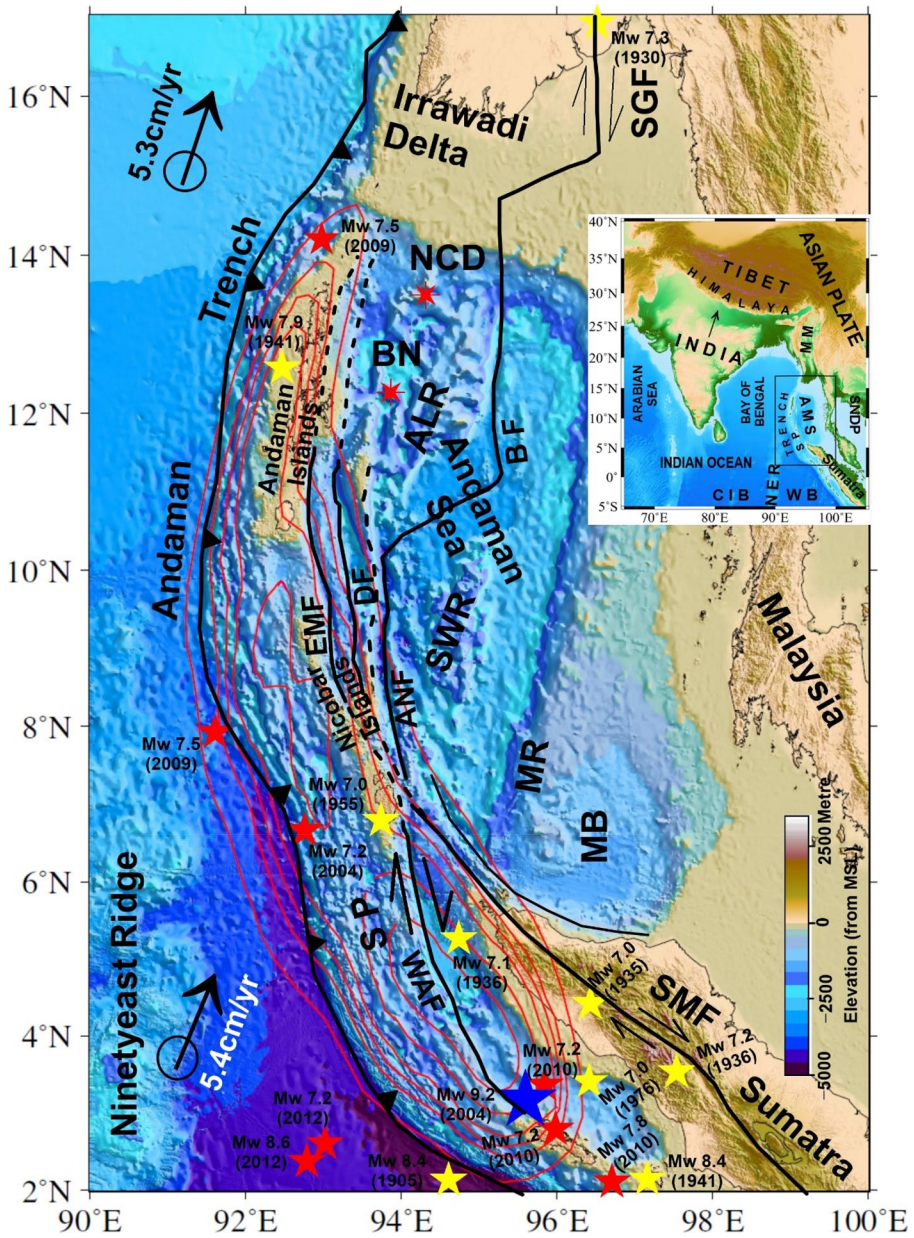


Fig. 1 Simplified map showing the tectonic framework of the Andaman–Sumatra margin (after Curray and Munasinghe 1991; Curray 2005; Radhakrishna et al. 2008). Inset: regional map of India–Eurasia collision zone, showing the position of Fig. 1 (framed rectangle). Contoured red lines show relative changes of released strain energy with respect to the position along the strike of the trench for 600 s since initiation of the rupture (the maximum contour value of unity is obtained after normalization; cf. Fig. 4 of Ishii et al. 2005); Stars: epicenters of major events (Yellow: pre-2004, and Red: post-2004) indicating magnitude and year; Black star with cross: positions of volcanic eruptions; circle with arrow: site for determination of the velocity vector of the Indian plate (after DeMets et al. 1994). *SP* sliver plate, *SNDP* Sunda plate, *BF* Boundary Fault, *AMS* Andaman Sea, *ANF* Andaman–Nicobar Fault, *DF* Diligent Fault; *EMF* Eastern Margin Fault, *WAF* West Andaman Fault, *SWR* Sewell Rise, *MR* Mergui Ridge, *SMF* Sumatra Fault, *SGF* Sagaing Fault, *ALR* Alcock Rise, *NER* Ninetyeast Ridge, *BN* Barren and *NCD* Narcondam

reveal recurrence of great earthquakes, including that in 2004, along this margin (Khan et al. 2018; Shamim et al. 2019). Our previous work has identified that the rupture migration of the 2004 mega-event was principally controlled by the along-strike segmentation and geometry of the subducting plate between Sumatra and Andaman (Khan et al. 2017 and references therein). Thus, the present study aims at understanding the occurrences and migration of seismicity vis-à-vis the deformation of both the underriding and overriding plates in the backdrop of the above discussed parameters.

The 2004 off-Sumatra mega-earthquake, which occurred after a time gap of 40 years since the incident of the March 28, 1964, M_w 9.2 Alaska earthquake, has drawn widespread attentions of the earth scientists, physicists and mathematicians globally and has remained in the focus of in-depth understanding for more than a decade (Ammon et al. 2005; Lay et al. 2005; Ishii et al. 2005; Meltzner et al. 2006; Dewey et al. 2007; Rajendran et al. 2007; Stein and Okal 2007; Rajendran et al. 2008; Gahalaut et al. 2010; Prawirodirdjo et al. 2010; Paul et al. 2012; Moeremans et al. 2014; Sevilgen et al. 2012; Henstock et al. 2016). The genetic link between the evolution of the Myanmar microplate toward north (cf. inset in Fig. 1), the 2004 mega-event (Ishii et al. 2005), critical obliquity of the Indian plate convergence ($20^\circ \pm 5^\circ$, McCaffrey 1992) and the development of the Mergui–Andaman basins toward south (Khan and Chakraborty 2005) led to a self-organized inclusive growth of the tectonic domain during the Late Cenozoic period (Maung 1987; Khan 2005). Segment-limited opening of different basins (Khan and Chakraborty 2005; Morley 2017), concentrated deformation (Khan 2007), generation of great earthquakes (Fig. 1), trenchward migration of seismicity under co- and post-seismic deformation phases (Shamim et al. 2019), 2004 seismic energy bursts with subsequent generation of tsunami (Ishii et al. 2005), co-seismic slip and vertical displacements (Ammon et al. 2005; Ishii et al. 2005; Lay et al. 2005; Subarya et al. 2006; Gahalaut et al. 2006; Chlieh et al. 2007), and widely variable trench-parallel stress perturbation (Shamim et al. 2019; Khan et al. 2020) are the motivating factors to delineate the lithospheric structure along the margin between the North Andaman Islands and the northwest Sumatra. Gravity modelings using free-air gravity anomalies along arbitrary profiles were carried out earlier (cf. Mukhopadhyay 1988; Mukhopadhyay and Krishna 1991, 1995; Radhakrishna et al. 2008) for segment-specific planar geometry of the subducting lithosphere along the Andaman–Nicobar region. The present study, based on joint analysis of the modeled geometry and topography, was aimed to delineate various tectonic structures along this plate margin. Forward gravity modelings were carried out along five trench-perpendicular profiles. The positions of these profiles were selected on the basis of the location of initiation of opening of the MB and Andaman Sea from northwest Sumatra, occurrences of major tectonic events, plate obliquity, 2004 earthquake rupture migration characteristics, 2004 earthquake-induced stress perturbation, and tectonic features of the overriding plate. The modeling was done on the basis of free-air gravity data for the underriding (oceanic) and overriding (continental) lithospheres. All the constraints have been addressed by analyzing the sensitivity of free-air gravity anomalies to the bending of Moho, the detailed structures of the underriding Indo-Australian plate and the overriding Eurasian continental lithosphere, the geometries of the fore-arc, Andaman Spreading Ridge (ASR), Mergui Ridge (MR), MB and Sewell Rise (SWR), and various continental as well as oceanic crustal elements.

The delineated structures of different tectonic features of this oceanic-continent collision boundary allow to assess the structural control on the dynamics and kinematics along the plate margin between the Myanmar and the Sumatra regions. The level of deformation in different segments of both the plates across the boundary assessed through the analysis of seismic activities and the seismic energy release characteristics would also be useful

for future hazard assessment of the region. We scrutinized the occurrences of earthquakes during the period 1976–2015, and compared these seismic activities in terms of different tectonic elements identified along the profiles. Relative release of seismic scalar moment (Kanamori 1977) with reference to the incident of the 2004 mega-event was also analyzed for the period 1976–2015 and compared with the tectonic elements. All the geodynamic and kinematic processes have been addressed in the backdrop of different tectonic elements.

2 Tectonic Setting

The tectonics of the northeastern margin of the Indian Ocean, dominated by the mutual interaction between a number of minor plates between the subducting Indo-Australian plate and the overriding Eurasian plate, was responsible for the development of the Java–Banda–Sumatra–Andaman–Burma subduction system, forming a continuous belt with a broad curvature toward southwest (Fitch 1972; Curray et al. 1979; Weissel et al. 1980; Mitchell 1981; Tapponnier et al. 1986; Hall 2002; Khan and Chakraborty 2005; Chakraborty and Khan 2009; Morley and Searle 2017). The major morphotectonic features along this plate margin include the abyssal plain (AP) of the Indian Ocean, the Ninetyeast Ridge (NER), oceanic rises such as the Alcock Rise (ALK) and Sewell Rise (SWR), the Java–Andaman Trench, the Andaman–Sumatra accretionary prism, active volcanoes of the island-arc system (e.g., Barren and Narcondam), the Andaman Sea spreading center, and back-arc basin (BAB) (Curray 2005; Morley and Alvey 2015; Clift 2017; Bandopadhyay 2017; Singh and Moeremans 2017) (Fig. 1). Two regional strike-slip faults in the tectonic province, the Sumatra Fault (SMF) in the south and the Sagaing Fault (SGF) in the north show dextral movements and created favorable conditions for the development of a pull-apart basin in the central part (the Andaman Sea basin; Fig. 1, Khan and Chakraborty 2005). The NNE–SSW trending NER, separating the Central Indian Basin from the Wharton Basin, has oblique intersection with the Andaman trench (Gordon et al. 1998; Krishna et al. 1999). The evolutionary history of the region started during the Early Cretaceous break-up of the Gondwanaland and northward movement of the Indian and Australian plates. These processes initiated the subduction related phenomena along the Western Sunda Arc, the development of the Java trench and formation of the volcanic-arc system (Curray 2005 and references therein). The accretionary prism was developed through continuous to intermittent accretion of sediments from Cretaceous to Eocene; associated deformation in the Andaman Islands took place from Eocene to Pliocene (Scotese et al. 1988; Clift, 2017; Bandopadhyay and Carter 2017). North to north–northeast migration of the Indo-Australian plate and its subduction beneath the south Asian/Myanmar microplate was accompanied by $\sim 20^\circ$ rotation of the Myanmar–Andaman–Sumatra trench-systems in late Paleocene (Patriat and Achache 1984; Curray 2005; Charusiri et al. 2006).

The trend of the Andaman–Sumatra subduction margin is NW–SE near the Sumatra region, but changes continuously to become almost N–S around the Nicobar–South Andaman margin in the central part (between 8° N and 12° N) and NNE–SSW in its northern part (beyond 12° N). This change from south to north is associated with the decrease in convergence rate of the Indo-Australian plate and increased northward obliquity of the plate margin with respect to the convergence direction (Lay et al. 2005).

The obliquity of the stress vector is partitioned into a complex stress system, which gave rise to the development of large fore-arc strike-slip faults paralleling the trench-arc system (e.g., the SMF, Fig. 1), trench-orthogonal underthrusting of the subducting plate (Fitch 1972; Diament et al. 1992), and a sliver plate, bounded by the trench of the subduction zone and the strike-slip fault (McCaffrey 1992). The partitioned trench-parallel and trench-orthogonal components are manifested by a variable deformation, both locally and regionally (McCaffrey 1993; McClay et al. 2004; Heuret and Lallemand 2005; Ramsey et al. 2007; Leever et al. 2011; Castelltort et al. 2012; McNeill and Henstock 2014; Guerit et al. 2016). Depending on the convergence obliquity along the plate margin, a population of faults is activated (Brune 2014), and convergence velocity facilitates trench migration (Schellart 2008), and compression or extension dominants in the areas from the back-arc to fore-arc (Kimura 1986; Bevis et al. 1995; Chemenda et al. 2000; Heuret et al. 2007). Convergence obliquity also influences the opening and modulation of sedimentary basin architecture (Saylor et al. 2010; Bennett et al. 2016) and other surface processes, like uplift and relief evolution (Guerit et al. 2016), leading to rotation with dextral stepovers opening a pull-apart basin (e.g., the Andaman Sea, Kamesh Raju et al. 2004; Morley 2017).

Great earthquakes along the Andaman–Sumatra margin were correlated with the segment-specific margin tectonics, but no earthquake of magnitude more than 8.0 was recorded near the Andaman–Nicobar region (Khan et al. 2018). The previous largest event of $M_W \sim 7.9$, accompanied by tsunami, occurred near the Nicobar Island in 1881, which was followed by 1941 $M_W 7.7$ Andaman earthquake (Kennett and Cummins 2005). The 2004 rupture shows significant along-strike variations of rupture velocity and slip with a maximum (~ 15 m) between Northern Sumatra and Nicobar and a second major slip of ~ 5 m near the Andaman region (Ammon et al. 2005; Catherine et al. 2005; Earnest et al. 2005; Jade et al. 2005; Lay et al. 2005; Gahalaut et al. 2006; Chlieh et al. 2007). The migrated stress also triggered swarm-type earthquake activities at certain locations near the north Andaman Island in December 2004 and near the Nicobar Island in January 2005 (Mishra et al. 2007a, b; 2011; Kamesh Raju et al. 2012; Kumar et al. 2016). Ishii et al. (2005) found a major burst of radiated energy near northwest Sumatra during the 2004 event and identified a second peak near the site of the 1881 $M_W \sim 7.9$ event, to the west of Car Nicobar Island. These strange tectonic settings and the evolving dynamics and kinematics require an in-depth understanding of the study area.

3 Data

We have used DTU15 gravity model (Andersen et al. 2016) for this work, along with topography (V18.1; Smith and Sandwell 1997) from global 1-min gridded data (cf. http://topex.ucsd.edu/cgi-bin/get_data.cgi). These extracted data have better accuracy compared to other gravity data acquired for academic work, but less accuracy than those acquired for exploration purposes (Sandwell et al. 2014). These satellite derived gravity anomaly data are more uniform and have good coverage for analyzing the regional gravity beneath the ocean floor. Although the resolutions of these data do not match the ship-borne gravity data for low wavelengths, these data compare well with ship-borne data for wavelengths more than 20 km to model the deeper oceanic features (Tiwari et al. 2003) and have an accuracy of ~ 5 – 10 mGal (Rapp 1998). The gravity fields in ocean regions correlate with the equipotential shape of the sea surface. This fact has been used while deriving the

free-air anomaly data from the measured sea heights using radar altimeters aboard satellites (Sandwell et al. 2014). Following these assumptions, no modifications were made on the sea surface heights during modeling along different profiles.

Initial densities of rock units constituting different tectonic elements and of the ocean water were taken from the studies of Dziewonski and Anderson (1981), Mukhopadhyay (1988), Radhakrishna et al. (2008) and Singh et al. (2008) (cf. Table 1). Farther east of the BAB, a density of 2700 kg m^{-3} has been selected initially for the transitional crust. Initial thicknesses of the oceanic lithospheres at five locations were derived using the half-space cooling model, $L = 2\sqrt{(kt)}$ (Fowler 2009), where L is the thickness of the lithospheric plate in km, t is the age of the subducting oceanic lithosphere in Ma for locations near trench along both the profiles (Müller et al. 1997), and k is the thermal diffusivity, taken as $10^{-6} \text{ m}^2 \text{ s}^{-1}$ for the present analysis. Thicknesses of different layers of the sediments and/or crusts, lying on the upper part of the lithosphere, were taken from the dataset of NOAA, United States of America (Divins 2003).

4 Methodology

4.1 Spectral Analysis and Estimation of Layer Parameters

The crust-mantle boundary along five profiles was derived by the spectral analysis of free-air gravity anomaly data (Figs. 2, 3). This technique is extensively used on potential field data to determine the depth of basement (Studinger et al. 1997; Ghosh and Singh 2014; Studinger and Miller 1999; Chamoli and Dimri 2010). The spectral analysis was done using MAGMAP module of Oasis Montaj software 8.4. To perform fast Fourier transform (FFT) of the gravity data, a square box of $2^\circ \times 2^\circ$ dimensions was applied from the edge of the selected profile, and the box was shifted by 1° each time up to the end of the profile; the results were overlapped for 1° in this process. Spectral analysis to estimate the depth of different subsurface interfaces from the gradient of the power spectrum at different wave number intervals was previously carried out by Spector and Grant (1970), Treitel

Table 1 Densities of different geological units for the initial and final models

Elements/blocks	Initial density (kg m^{-3})	References	Final density (kg m^{-3})
Sea water	1030	Radhakrishna et al. (2008)	1030
Sediment	2400	Radhakrishna et al. (2008)	2400
Transitional crust	2700	Dziewonski and Anderson (1981)	2800
Oceanic crust	2900	Mukhopadhyay (1988)	2900
Lithospheric mantle	3300	Radhakrishna et al. (2008)	3350
Asthenosphere	3235	Dziewonski and Anderson (1981)	3250
Andaman Spreading Centre	3290	Mukhopadhyay (1988)	3250
Sewell rise	2600	Radhakrishna et al. (2008)	2600
Ninety east ridge	2950	Radhakrishna et al. (2008)	2950
Alcock rise	2600	Mukhopadhyay (1988)	2600
East basin	2600	Radhakrishna et al. (2008)	2600

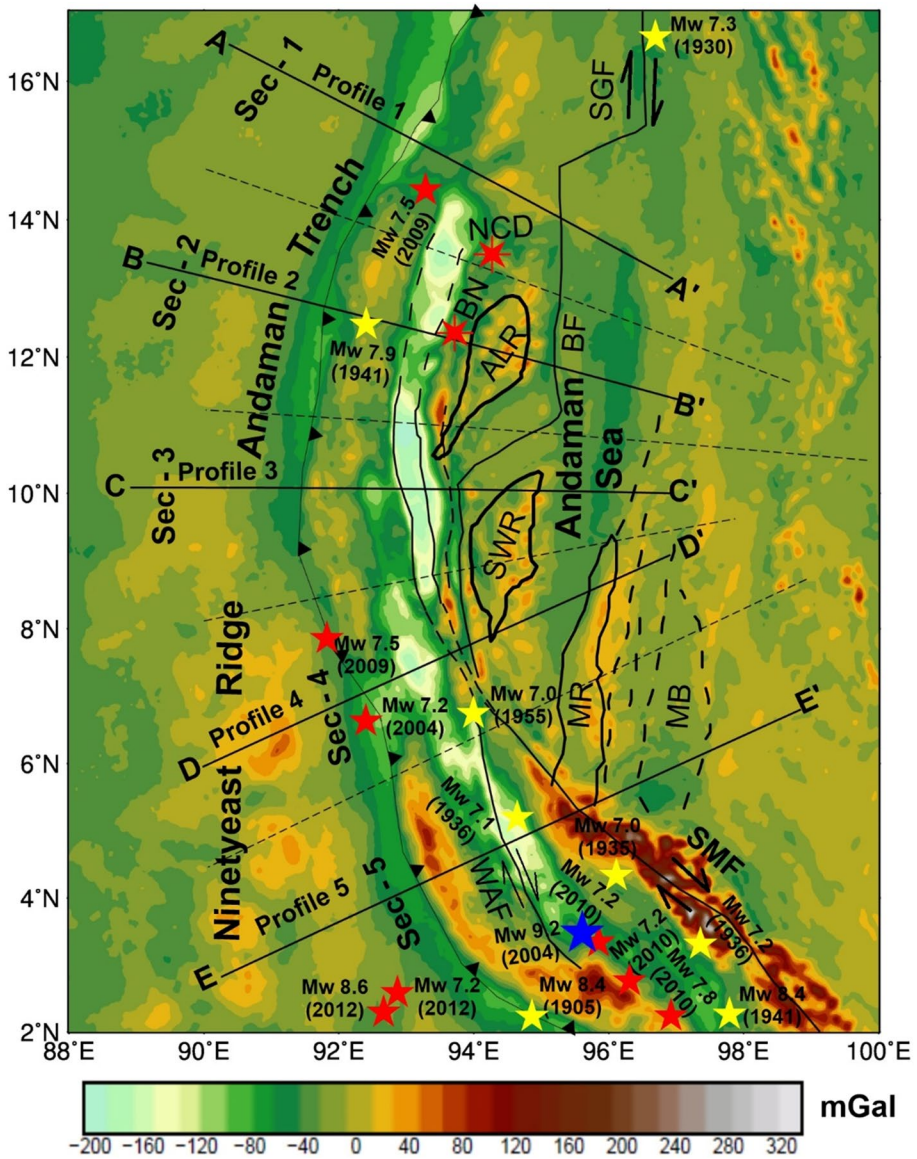


Fig. 2 Shaded free-air anomaly map of the study region. *MB* Mergui Basin. *AA'*, *BB'*, *CC'*, *DD'* and *EE'* are five profiles considered for gravity modeling of the convergent margin. Other annotations are explained in Fig. 1

et al. (1971) and Hahn et al. (1976). The linear segment of the power spectrum of gradient dI (Fig. 4), corresponding to lower frequency interval, is associated with the Moho, a layer of maximum density contrast along the crust-mantle boundary. The linear segments with intermediate and higher frequency intervals correspond to shallower interfaces of different oceanic sedimentary layers. Different depths of interfaces with distinct density contrast are determined by the following equation:

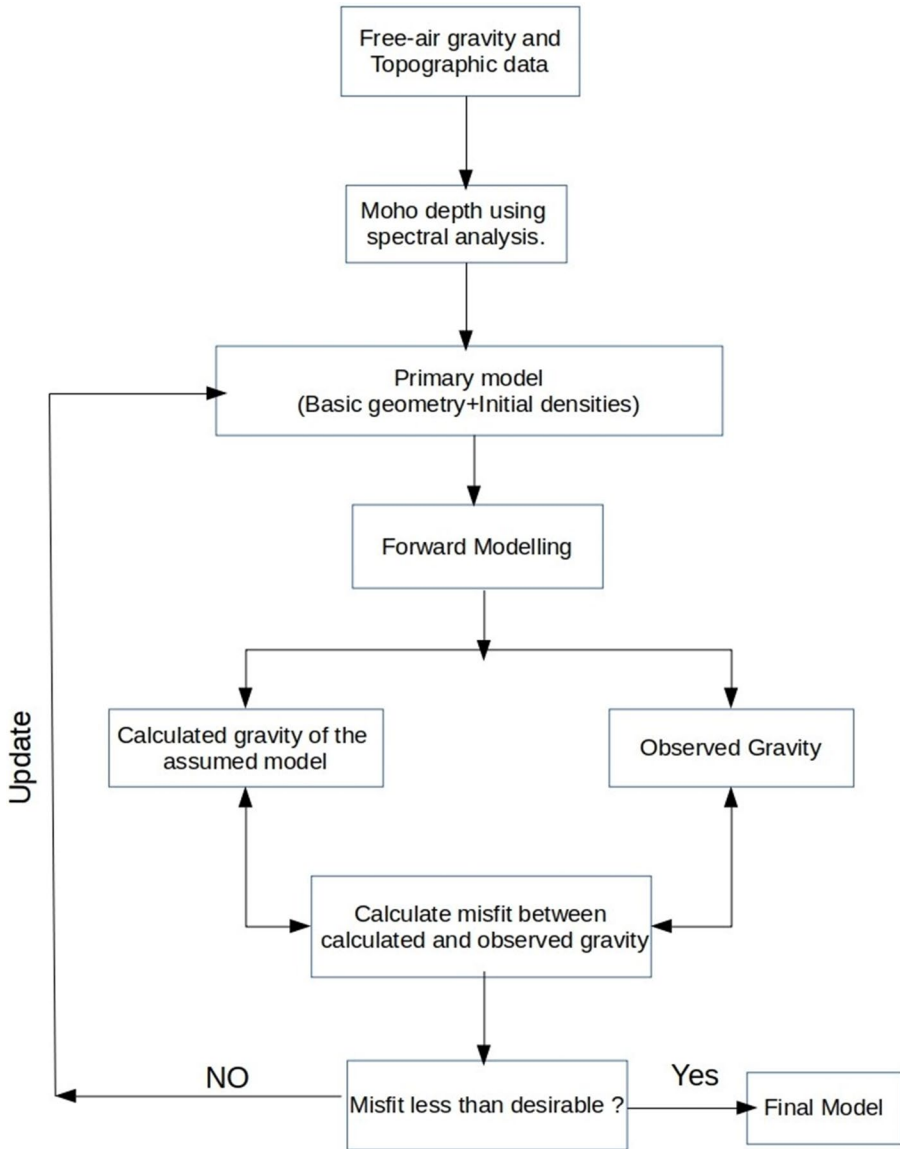


Fig. 3 Flowchart showing the various steps followed for the gravity modeling

$$|d| = \frac{-1}{4\pi} \left[\frac{\log E_1 - \log E_2}{k_1 - k_2} \right]$$

where d is the depth to the mean interface, E_1 and E_2 are the power spectrum at wavenumber k_1 and k_2 (cf. Indriana 2008; Spector and Grant 1970; Karner and Watts 1983; Maus and Dimri 1995; Chamoli and Dimri 2010; Bansal and Dimri 2010). The term in the square bracket is actually the slope of the segments between wavenumber k_1 and k_2 .

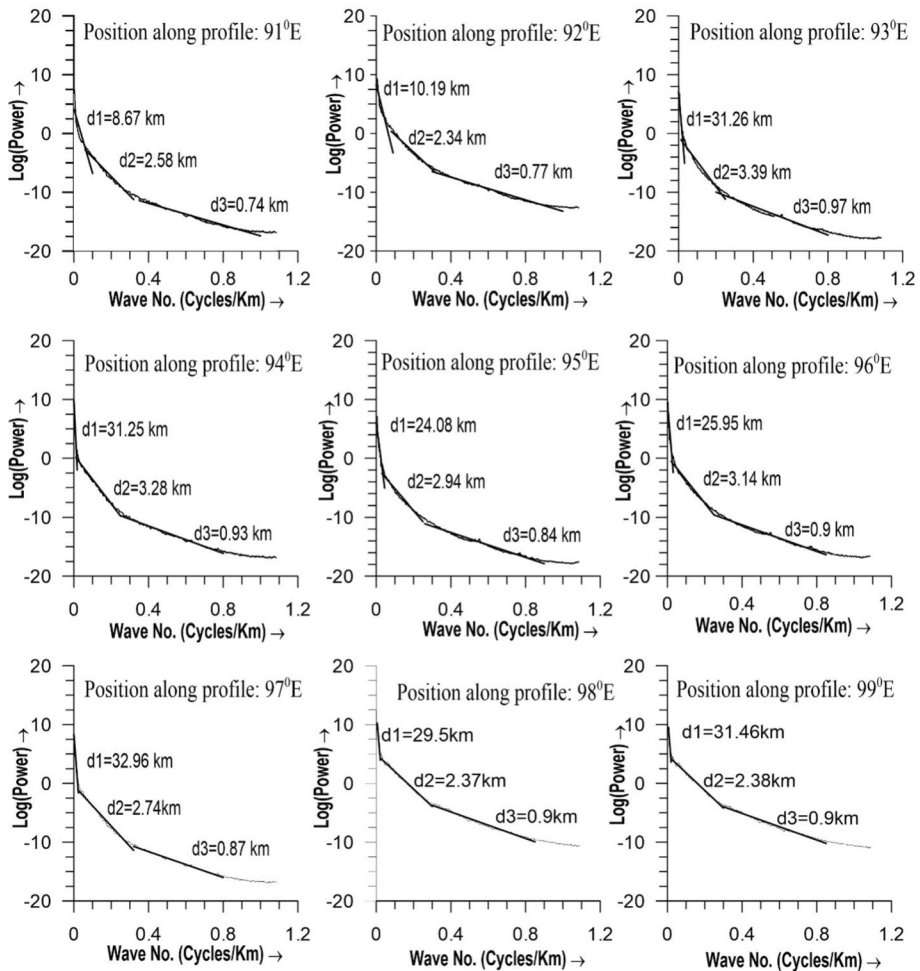


Fig. 4 Illustrative plots of spectral analysis results for the profile AA' passing through L profile-3 (Sector 3 in Fig. 1). $d1$ is the depth of the Moho

4.2 Gravity Modeling

The Andaman–Sumatra margin is purely oblique with respect to the convergent vector of the Indo-Australian plate; the trench, passing through this area, is curved with local variations in curvatures toward north and south near 15° N and 7° N latitudes. Other tectonic features were evolved along this margin during the Late Cenozoic, partially following the margin geometry. The locations of the five gravity profiles were selected on the basis of the plate obliquity, structural discontinuity, 2004 earthquake induced stress perturbation and associated rupture migration. These five profiles are passing through important tectonic features such as NER, West Andaman fault (WAF), Andaman Spreading Centre (ASC), fore-arc, back-arc, inner arc volcanics and Mergui Terrace. The locations of the profiles are also predominantly decided by the opening and spreading of the Andaman Sea (Khan and Chakraborty 2005), occurrences of great earthquakes and rupture propagation of the

2004 M_w 9.2 Sumatra earthquake (Bilham 2005; Ishii et al. 2005). The configuration of the Mohorovičić discontinuity (Moho) was derived by spectral analysis of the gravity data (Tselentis et al. 1988; Studinger et al. 1997; Ghosh and Singh 2014; Studinger and Miller 1999; Chamoli and Dimri 2010). Using the value of lithospheric thickness (Fowler 2009), density, Moho depth and dimensions of different sedimentary layers (Divins 2003), the preliminary model was constructed using Geosoft Oasis Montaj 8.4. Gravity forward modeling was applied for the calculation of gravity effects of a given density distribution. Gravity forward modeling (GFM) calculation of gravitational field for a given density distribution is extensively used for the exploration of the Earth's interior (Wieczorek 2007). The position and bending of the lithosphere were constrained by the Benioff zone trajectories along the five profiles (Khan and Chakraborty 2005; Chakraborty and Khan 2009). The distributions of earthquake foci on the vertical cross section were used to demarcate the Benioff zone as well as the extent of the subducting plate inside the mantle (Cardwell and Isacks 1978; Furlong et al. 1982; Ruff and Kanamori 1983; Christova 2004). The distribution of hypocenters was worked as a constraint to model the bending part of the subducting plate. The structure of the subducting plate was drawn iteratively along the best fit line between the observed and computed data outlined by the earthquake foci (Mukhopadhyay and Dasgupta 1988; Lücke and Arroyo 2015). A uniform lithosphere thickness was determined by the half-space model discussed in Sect. 3. Information about other blocks (e.g., inner and outer arc volcanics, back-arc and fore-arc) to the east of the trench was compiled from Chakraborty and Khan (2009).

The GM-SYS, a forward modeling software, was used to create an initial model and set other parameters (e.g., density in the case of gravity modeling) by calculating the real-time gravity response of the created model (cf. Talwani et al. 1959; Talwani and Heirtzler 1964). The response was compared with the response of the observed gravity based on sensitivity test by changing geometries and densities of different tectonic domains (Herczeg et al. 2016), and by analyzing the misfit between observed and calculated data. In the present study, a density change of 0.01 gm/cc has been included at every iteration of the modeling. This software also uses 2D flat earth model, extending the profile from minus infinity to plus infinity to eliminate the edge effects. Basic initial model was generated, followed by subsequent modification of different layer thicknesses and densities, which have decreased the misfit between the calculated and observed data. While modification of the initial model was being carried out, other models suggested by Dessa et al. (2009), Singh et al. (2012), Singh et al. (2013) and Moeremans and Singh (2015) were also considered to constraint the thicknesses of the sedimentary layers. It may be mentioned here that the present result regarding the Moho depth obtained from the spectral analysis matches with the Moho depth of ~18–20 km given by Singh and Moeremans (2017) for the Andaman–Nicobar region. Subsequently, densities and geometries (e.g., thicknesses of the lithosphere, crust, fore-arc, back-arc, etc.) of different tectonic elements were modified through various steps of the iteration process (Fig. 3) to obtain reasonable models along the profiles (Figs. 5, 6, 7, 8, 9). At each iteration, the fit between the observed and calculated responses was estimated through minimization of error, and the final model was selected when r.m.s. error reduced to less than 5.0 mGal (i.e., 3.411 mGal for profile 1, 5.315 mGal for profile 2, 3.844 mGal for profile 3, 4.3 mGal profile 4 and 6.309 mGal for profile 5).

4.3 Seismic Activities and Moment Energy Release

Earthquake data for the region, between latitude 2° – 17° N and longitude 90° – 100° E, having magnitude $M_W > 4.0$ for the period from January 1, 1976 to December 31, 2015, were compiled from the USGS catalogue. Seismic activities under both pre- (i.e., January 1, 1976, to December 25, 2004: pre-12/04, Fig. 10a), co- (December 26–31, 2004, Fig. 10b) and post-seismic (January 01, 2005, to December 31, 2015: post-12/04, Fig. 10c) deformation phases were analyzed. Studies on the basis of teleseismic data for relocation illustrate that all locations are well computed only in relative sense (Engdahl et al. 1998, 2007; Engdahl and Villaseñor 2002; Pesicek et al. 2010). It was also noted that using similar type of data archived from different organizations, several workers have reconstructed the Benioff zone trajectories in drawing the upper boundary of the subducting slab (Cardwell and Isacks 1978; Furlong et al. 1982; Ruff and Kanamori 1983; Ponko and Peacock 1995; Gudmundsson and Sambridge 1998; van Keken 2003; Christova 2004; Heuret and Lallemand 2005; Kennett and Cummins 2005). Hence, within the constraint of available seismic database, hypocenters of all the events were separated for pre-12/04, co-seismic and post-12/04 phases and projected on the five reconstructed gravity models (Figs. 11, 12, 13, 14, 15). The relative changes of deformations of the different segments along the margin have been analyzed against the backdrop of apparent concentration and relative migration of seismic activities in space and time. Figure 1 shows that the large magnitude earthquakes are not uniformly distributed, but concentrated around the Sumatra margin, and few with lesser magnitude are located around the north Andaman area. These uneven distributions of epicenters of great earthquakes motivate us to examine the spatial distribution of seismic moment energy under both pre-12/04, co- and post-12/04 seismic phases more carefully (Fig. 16). Release in moment energy was computed over $1^{\circ} \times 1^{\circ}$ grids for the entire region. A moving grid window of dimension $0.5^{\circ} \times 0.5^{\circ}$ was selected during calculation to maintain inherent continuity of the data points. The log value of each seismic moment was projected at the crossing point of both the diagonals of each square-grid. Thus, a total of 651 point values were used for preparing the contour plot of seismic moment release (Fig. 16). We also compare our results with geodetic observations found by Subarya et al. (2006), Chlieh et al. (2007), Lorito et al. (2010) and Prawirodirdjo et al. (2010),

5 Results

5.1 Gravity Anomaly

The free-air gravity anomaly map of the study area (Fig. 2) shows a maximum contour value of ~ 480 mGal, contour value of ~ 20 – 80 mGal associated with the NER and the minimum gravity contour of ~ -200 to -120 mGal located in the area between the fore-arc and volcanic-arc; the latter possibly coincides with the zone of maximum bending of the descending lithosphere (Figs. 2, 5, 6, 7, 8, 9). The free-air anomaly drops steeply from ~ 60 mGal to ~ -50 mGal over a distance of 100 km toward east, past the fore-arc region, and further reduces to less than -160 mGal toward the volcanic-arc area. We interpret this to be the result of a thick sedimentary layer deposited above the sharp bending segment of the subducting Indian lithosphere below the fore-arc, where the Moho depth has increased rapidly (Figs. 5, 6, 7, 8, 9). These high negative free-air anomalies are typically observed along subduction zones. The Andaman–Nicobar–Sumatra trench is associated

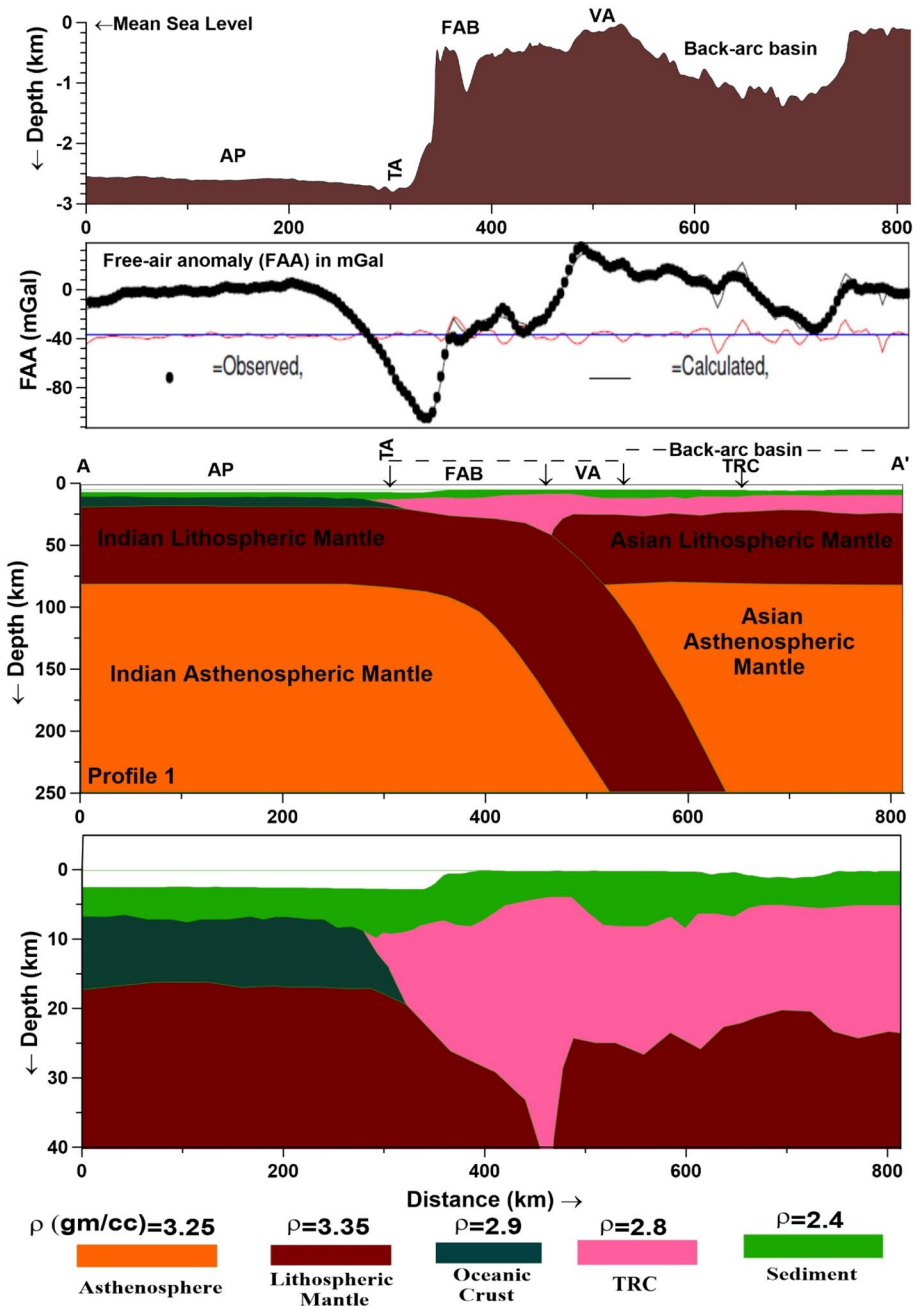


Fig. 5 Plots showing the 2D gravity modeling with topography along profile-1, across the Andaman–Sumatra plate margin. **a** Elevation along the profile, **b** free-air gravity anomaly along the profile, **c** model involving lithosphere and asthenosphere up to 250 km depth and **d** model showing details of the lithosphere up to 40 km depth. *AP* abyssal plain, *BAB* back-arc basin, *FAB* fore-arc basin, *TA* trench axis, *TR* trench, *TRC* transitional crust, *VA* volcanic arc. Index at the bottom shows the density values against the layers

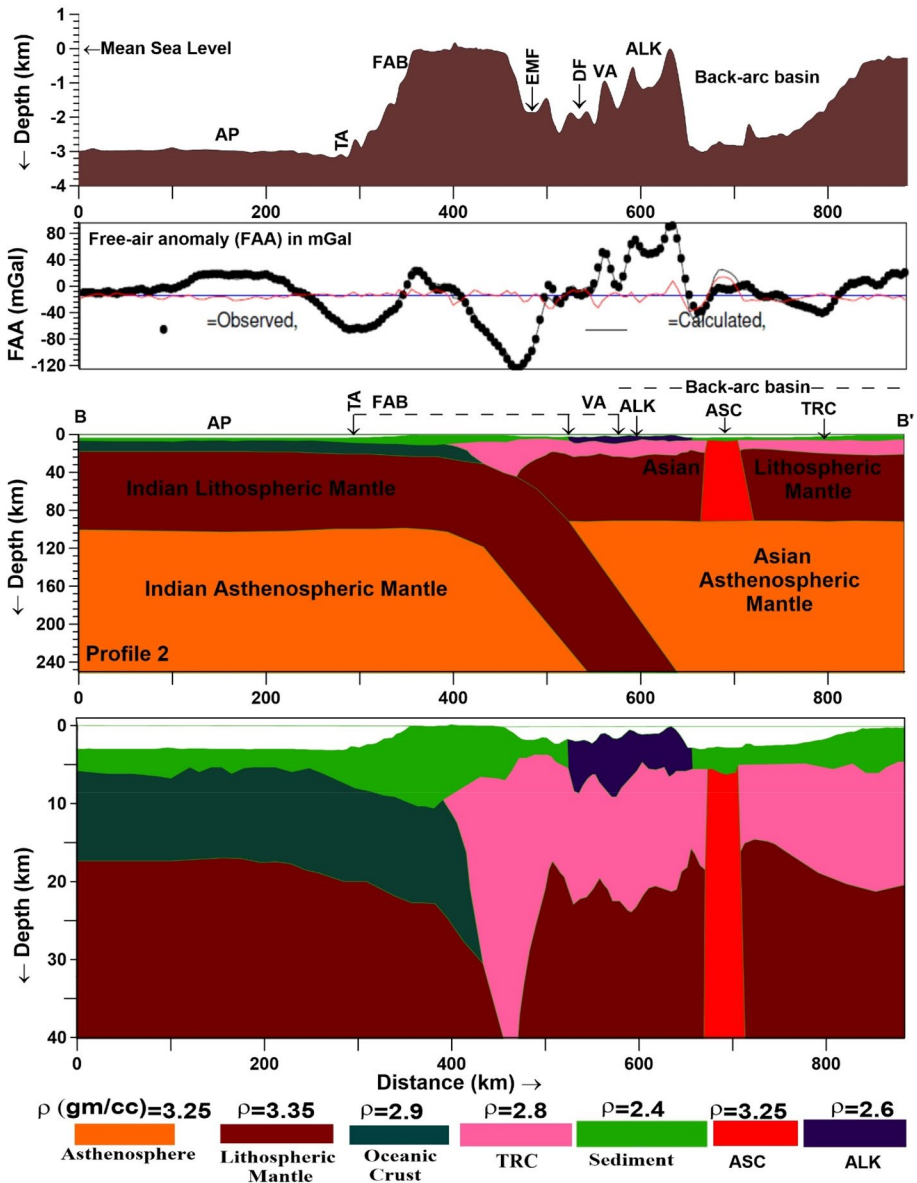


Fig. 6 Plots showing the 2D gravity modeling with topography along profile-2, across the Andaman–Sumatra plate margin. **a** Elevation along the profile, **b** free-air gravity anomaly along the profile, **c** model involving lithosphere and asthenosphere up to 250 km depth and **d** model showing details of the lithosphere up to 40 km depth. *ALK* Alcock Ridge, *AP* abyssal plain, *BAB* back-arc basin, *FAB* fore-arc basin, *TA* trench axis, *TR* trench, *TRC* transitional crust. Index at the bottom shows the density values against the layers

with a free-air gravity value of ~ -80 to -40 mGal. Concentrated high positive free-air anomalies (~ 120–320 mGal) are recorded in the adjacent area along the Sumatra sliver plate and the Sumatra fault (McCaffrey 1992). Scattered high anomalies are also found

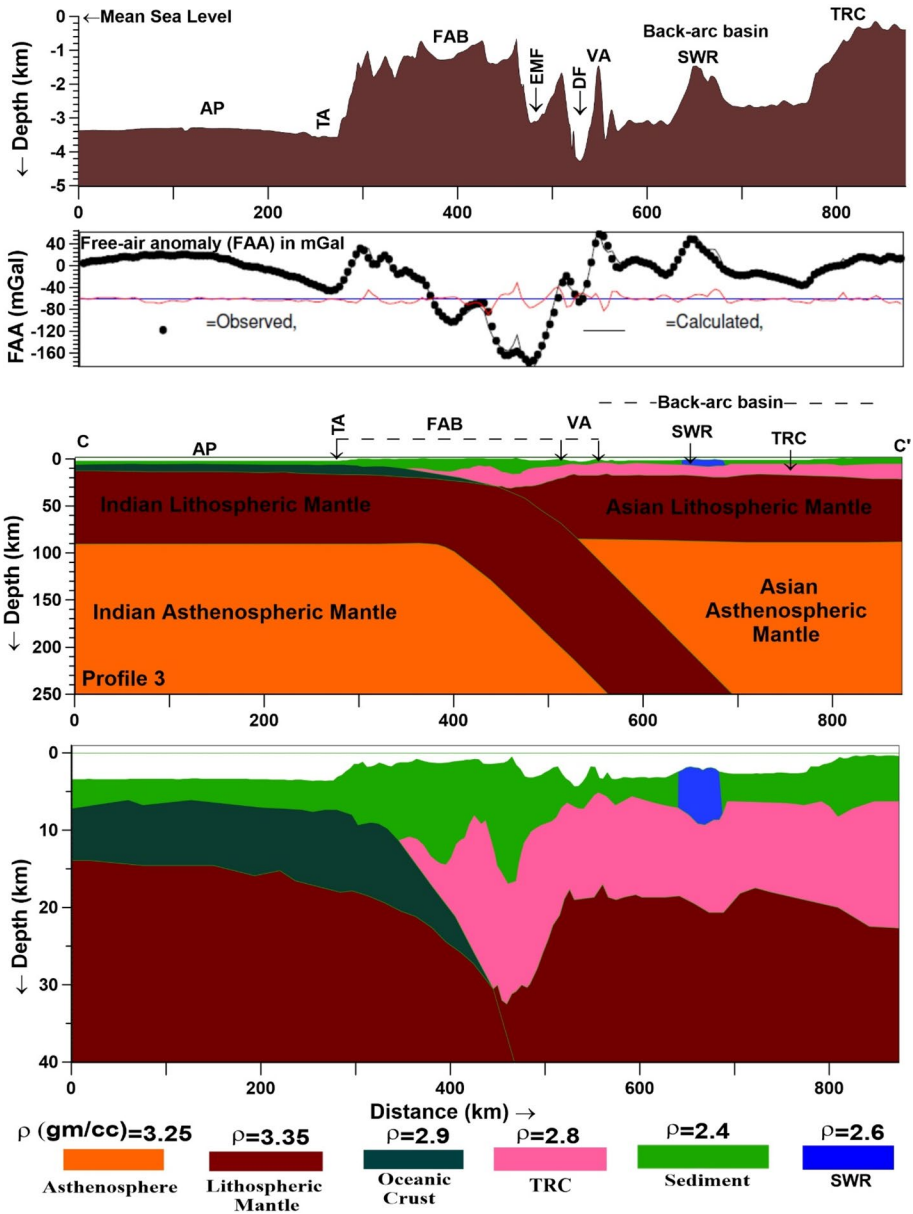


Fig. 7 Plots showing the 2D gravity modeling with topography along profile-3, across the Andaman–Sumatra plate margin. **a** Elevation along the profile, **b** free-air gravity anomaly along the profile, **c** model involving lithosphere and asthenosphere up to 250 km depth and **d** model showing details of the lithosphere up to 40 km depth. *AP* abyssal plain, *BAB* back-arc basin, *FAB* fore-arc basin, *SWR* Sewell Rise, *TA* trench axis, *TR* Trench, *TRC* transitional crust. Index at the bottom shows the density values against the layers

over the Alcock, Sewell seamounts and Mergui Ridge. Apparently younger age (~47 Ma) of the subducting oceanic lithosphere in this area (cf. Müller et al. 1997; Jacob et al. 2014) compared to that of the northern and southern segments of the Andaman–Sumatra margin

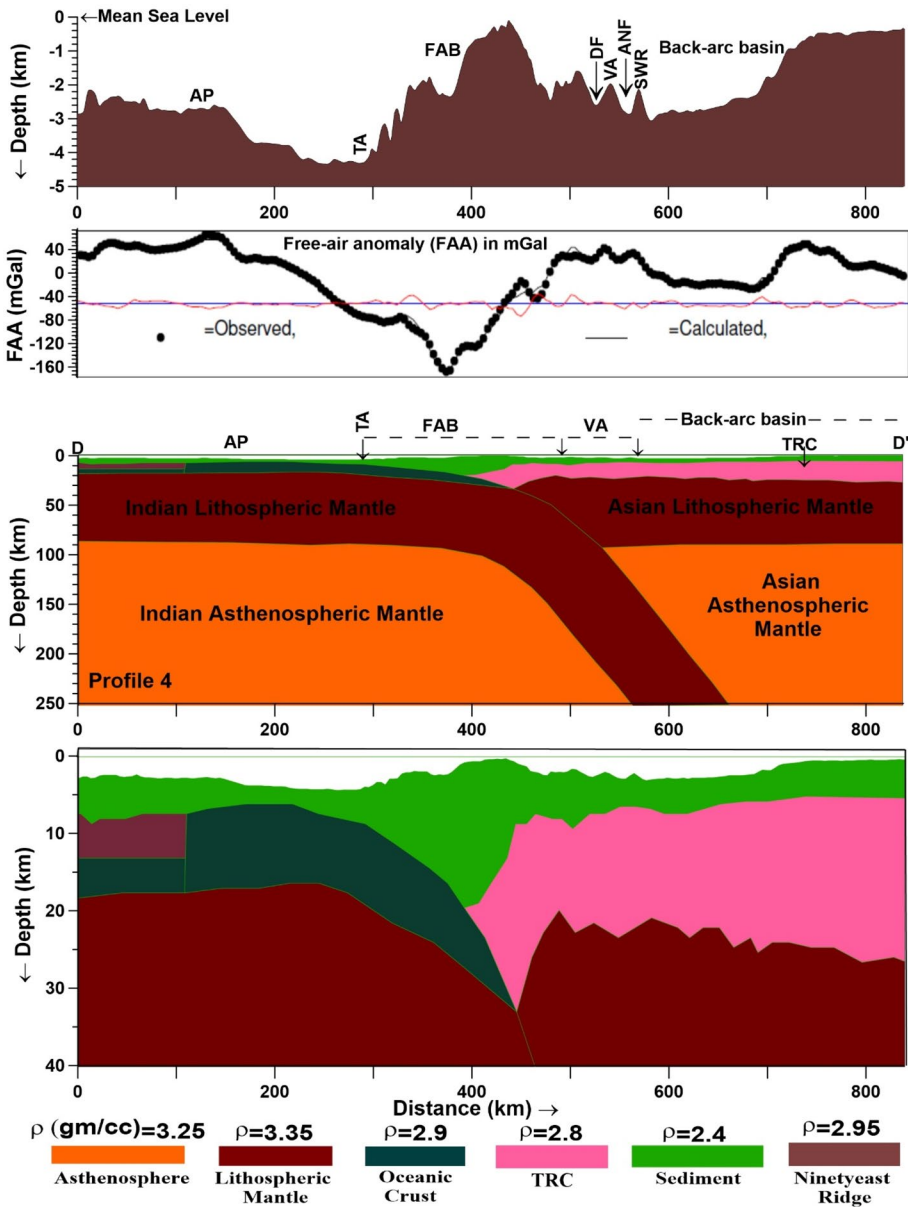


Fig. 8 Plots showing the 2D gravity modeling with topography along profile-4, across the Andaman–Sumatra plate margin. **a** Elevation along the profile, **b** free-air gravity anomaly along the profile, **c** model involving lithosphere and asthenosphere up to 250 km depth and **d** model showing details of the lithosphere up to 40 km depth. *AP* abyssal plain, *BAB* back-arc basin, *FAB* fore-arc basin, *SWR* Sewell Rise, *TA* trench axis, *TR* trench, *TRC* transitional crust. Index at the bottom shows the density values against the layers

indicates a thinned crust over the high-density mantle material, which is the possible cause for high gravity contrast. The abyssal plain (Figs. 2, 5, 6, 7, 8, 9) along the Andaman–Nicobar–Sumatra region is associated with moderate positive free-air anomaly (~0–30 mGal).

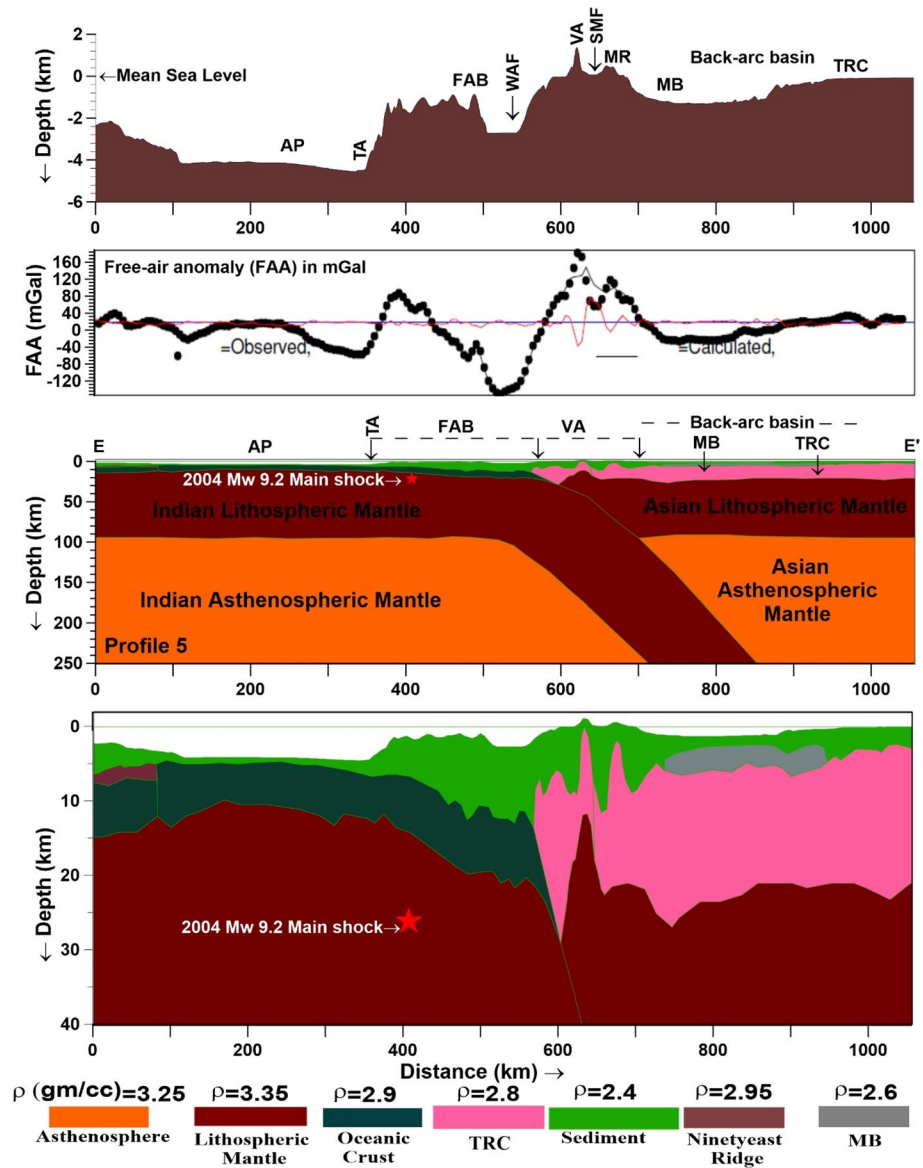


Fig. 9 Plots showing the 2D gravity modeling with topography along profile-5, across the Andaman–Sumatra plate margin. **a** Elevation along the profile, **b** free-air gravity anomaly along the profile, **c** model involving lithosphere and asthenosphere up to 250 km depth and **d** model showing details of the lithosphere up to 40 km depth. *AP* abyssal plain, *BAB* back-arc basin, *MB* east basin, *FAB* fore-arc basin, *SWR* Sewell Rise, *TA* trench axis, *TR* trench, *TRC* transitional crust. Index at the bottom shows the density values against the layers

The 2D-forward gravity models delineate the high-resolution geometries of the NER, trench (T), AP, fore-arc high (FAH), fore-arc basin (FAB), BAB, ASC, SWR, MR, MB,

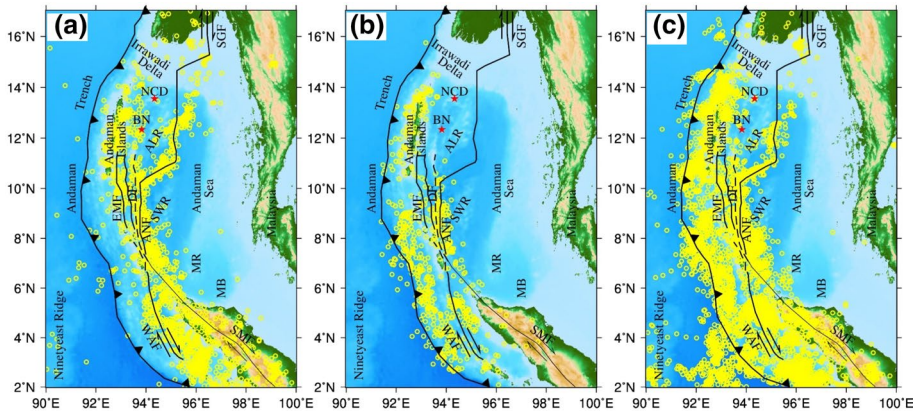


Fig. 10 Maps illustrating the distributions of earthquakes of magnitude M_w 4.0 and above under pre- (a i.e., January 1, 1976, to December 25, 2004), co- (b December 26–31, 2004) and post-seismic (c January 01, 2005, to December 31, 2015) deformation phases. The abbreviated annotations are explained in the caption of Fig. 1

transitional crust (TRC), continental crust (CC), the Moho and lithosphere–asthenosphere boundary (cf. Figs. 5, 6, 7, 8, 9, 11).

The profile 1 is located on the northernmost part (sector 1) of the study area, to the south of the Irrawadi delta (Figs. 2, 5). The gravity value of ~ 10 mGal is associated with the abyssal plain. A large negative value of gravity (~ -110 mGal) is found to be associated with the fore-arc basin. The volcanic arc (VA), on eastern side of the FAB, accounts for positive gravity anomaly as high as $+40$ mGal. A sharp decrease in the anomaly from ~ 25 to 0 mGal is associated with the back-arc basin. A little deformed TRC and shallow-deposited sediment beneath the back-arc basin turns the gravity anomaly toward the low value. The thickness of the oceanic crust on the subducting lithosphere is about 10 km. The lateral extension of the FAB is about 155 km. The overriding plate is found to be associated with denser thickened transition crust (TRC) accounting for the positive gravity anomaly. The sediment thickness is reasonably high (> 5 km) in the FAB.

The profile 2 passes through the ALK and ASC at latitude $\sim 13^\circ$ N in sector 2 (Figs. 2, 6). A little positive gravity value as high as 20 mGal is found to be associated with the deformed oceanic crust beneath the AP (Moeremans et al. 2014). A sharp decrease in gravity value (up to -75 mGal) accounts for increase in the thickness of the sediment in the trench area as well as the FAB. A further increase in gravity value to more than 30 mGal might have been caused by the presence of a sliced oceanic crust thrust up to a shallow level. A large negative value of gravity (-120 mGal) further east is associated with comparative low-density (2.8 gm/cc) thickened TRC, up to more than 40 km depth (Fig. 6). This possibly happened because of a deeper depth of Moho of the subducting plate below the VA. The positive gravity value toward east is found below the VA, but the trend has a disturbed pattern caused by the presence of a series of faults located between the VA and the trench. The faults also affect the overall topographic of the VA. Scattered gravity values as high as 95 mGal are observed around the location of ALK seamount, whereas a little low gravity of -40 mGal is found near the ASC. The thickness of the subducting oceanic crust is estimated to be ~ 10 km, whereas the thickness of sediment increases to more than 10 km beneath the extended (~ 230 km) FAB.

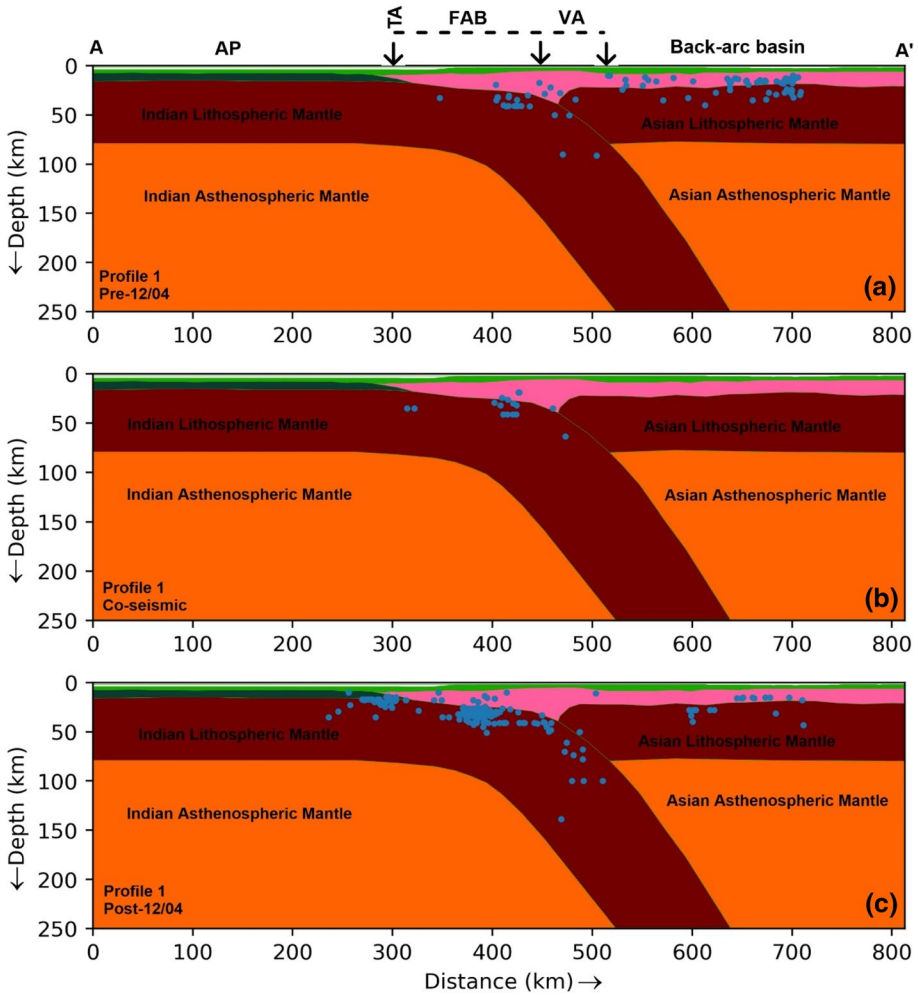


Fig. 11 Depth sections showing the distributions of earthquakes in different tectonic units along profile 1 of sector 1 under pre- (a), co- (b) and post-seismic (c) deformation phases

The profile 3, selected at 10° N latitude in the Central Andaman region (i.e., sector 3), passes through the SWR (Figs. 2, 7). A high gravity value (~25 mGal) around the AP is found to be associated with thinner (~7 km) oceanic crust with shallow-level Moho. Further, toward east, the gravity values decreases and becomes minimum (~−185 mGal) below the FAB, which is possibly caused by the combined effect of thickened upper crust by tectonic accretion of low-density sediment. The shallow-level Moho and thickened TRC raise the gravity value of ~60 mGal over a narrow VA. The gravity value decreases below the back-arc basin with slight local positive value over SWR. The lateral extension of the FAB in this sector is anomalously high (~240 km). The estimated wide extension of the FAB complies with the results of earlier seismic study of Singh and Moeremans (2017).

The profile 4 passes through an area between SWR and MB where the trench axis takes a sharp turn toward north–south direction (Figs. 2, 8). The deformed thin sediment layer,

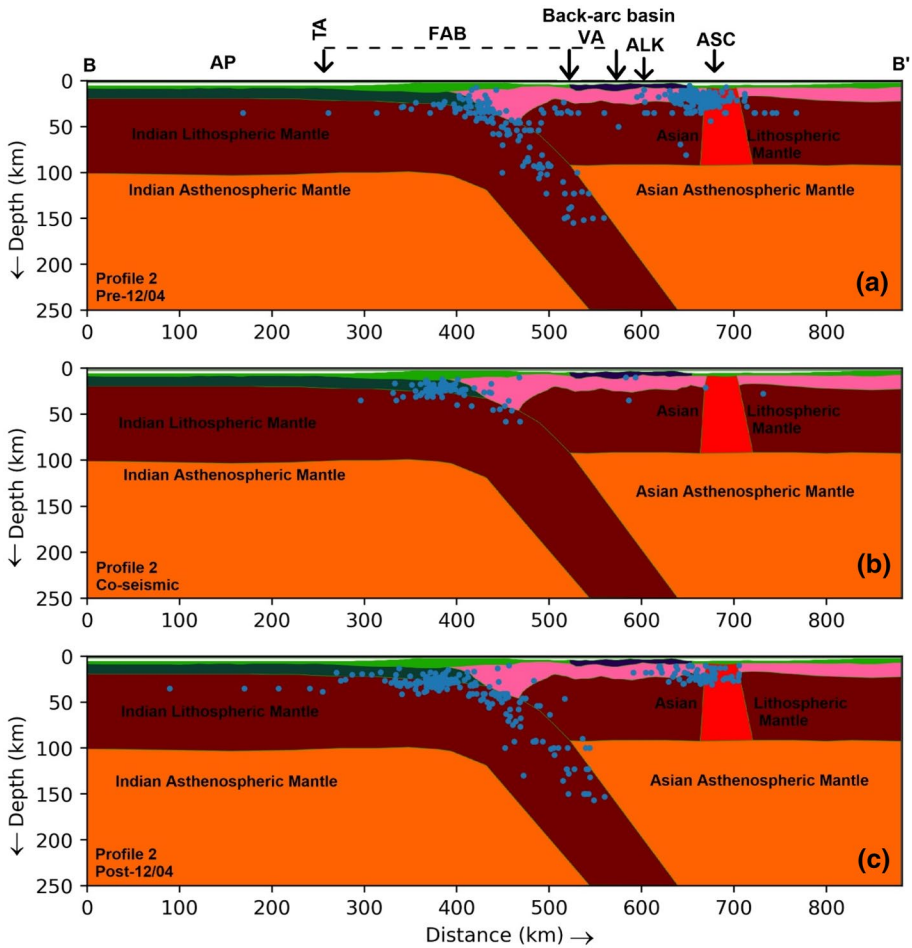


Fig. 12 Depth sections showing the distributions of earthquakes in different tectonic units along profile 2 of sector 1 under pre- (a), co- (b) and post-seismic (c) deformation phases

oceanic crust and the NER in the area of AP jointly raise the gravity anomaly to as high as 80 mGal. A sharp decrease in the gravity value to about -170 mGal in the trench area, and the FAB is due to the thickened sediment layer below the FAB developed by thrusting and tectonic accretion. Here, the lateral extension of the FAB is reduced to ~ 150 km. The positive gravity value of maximum ~ 40 mGal is associated with the VA. The gravity value remains low over the back-arc basin.

The profile 5 was taken across MB and NW Sumatra at latitude 4° N in sector 5. Two basins (e.g., Mergui, Andaman) were opened and the subducting plate recorded a critical plate obliquity in this area (McCaffrey 1992). The shallowly dipping plate in this sector presumably accounts for a major deformation of both the oceanic crust and lithospheric mantle (Figs. 2, 9). While the thinned sediment of ~ 1 – 2 km and oceanic crust of ~ 8 km are associated with zero gravity value surrounding the AP, the trench and FAB account for a reduced gravity value adjacent to the AP. Local positive gravity below the outer part of the FAB is possibly caused by thrusting of a part of the oceanic crust of the subducting plate

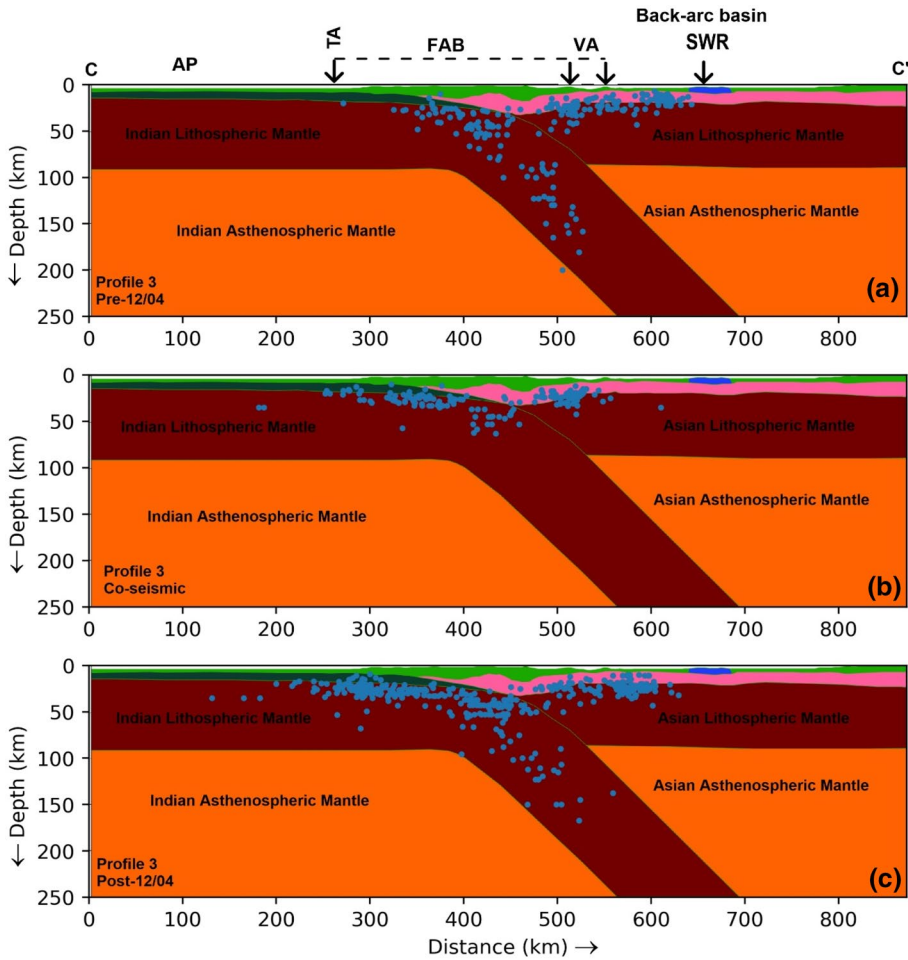


Fig. 13 Depth sections showing the distributions of earthquakes in different tectonic units along profile 3 of sector 1 under pre- (a), co- (b) and post-seismic (c) deformation phases

to a shallower level. A minimum gravity value of ~ -150 mGal can be explained by a thick layer of sedimentary prism and a deeper Moho below the inner part of the FAB. A high gravity of ~ 180 mGal is found to be associated with the VA. Intruding TRC through the sediment and the Asian lithospheric mantle causes this large gravity value. The sediment in the Mergui Basin accounts for a negative gravity of -30 mGal. This further increases to zero value toward east. The FAB is laterally extended by about 215 km, presumably suffered strong deformation in this sector 5 near NW Sumatra.

5.2 Distribution of Seismicity

Analysis of seismicity during pre-12/04 phase shows the occurrences of earthquake along a band paralleling the trench axis little away toward the east; the Andaman Sea spreading

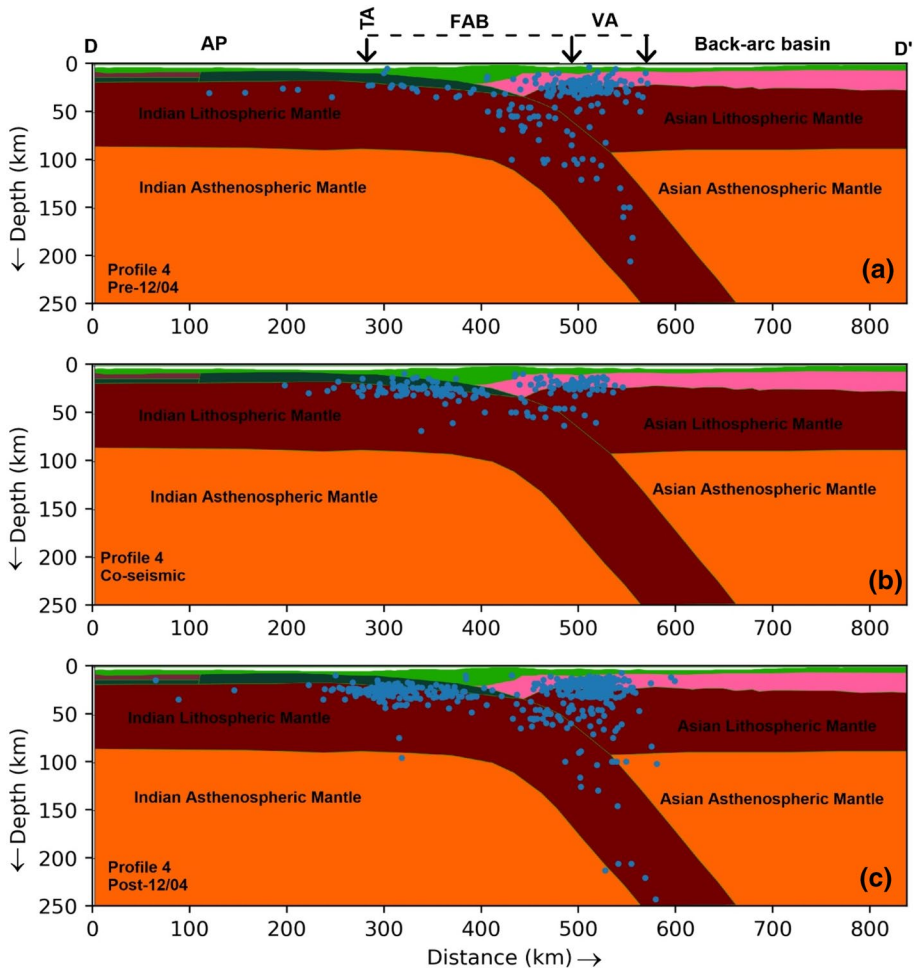


Fig. 14 Depth sections showing the distributions of earthquakes in different tectonic units along profile 4 of sector 1 under pre- (a), co- (b) and post-seismic (c) deformation phases

Ridge, connecting the SGF in the north and SMF in the south, shows quite phenomenal seismicity (Fig. 10a). Sporadic seismicity is also noted near the NER. Co-seismic deformation phase shows the concentration of earthquakes near the trench, apparently associated with three main clusters at $\sim 2^{\circ}$ – 6° N, $\sim 6^{\circ}$ – 10° N and $\sim 10^{\circ}$ – 14° N (Fig. 10b). A second band of seismicity of this phase is also found around $\sim 6^{\circ}$ – 10° N, near the ANF and EMF. These confined deformations in different segments along the margin might be related to the history of seismic slip of the 2004 mega-event (Subarya et al. 2006; Chlieh et al. 2007; Bletery et al. 2016). Prawirodirdjo et al. (2010), based on geodetic observation, also found similar segmented mega-thrust zones along the margin during the 2004 mega-event. Kuchay et al. (2015) also found shallow-level segment-specific distribution of seismicity and associated deformation pattern in this area, while Lorito et al. (2010) found the rupture migration of 2004 mega-event associated three main slip-patches with a maximum near the NW Sumatra. The stress perturbation (Khan et al. 2020) and the geometry of the

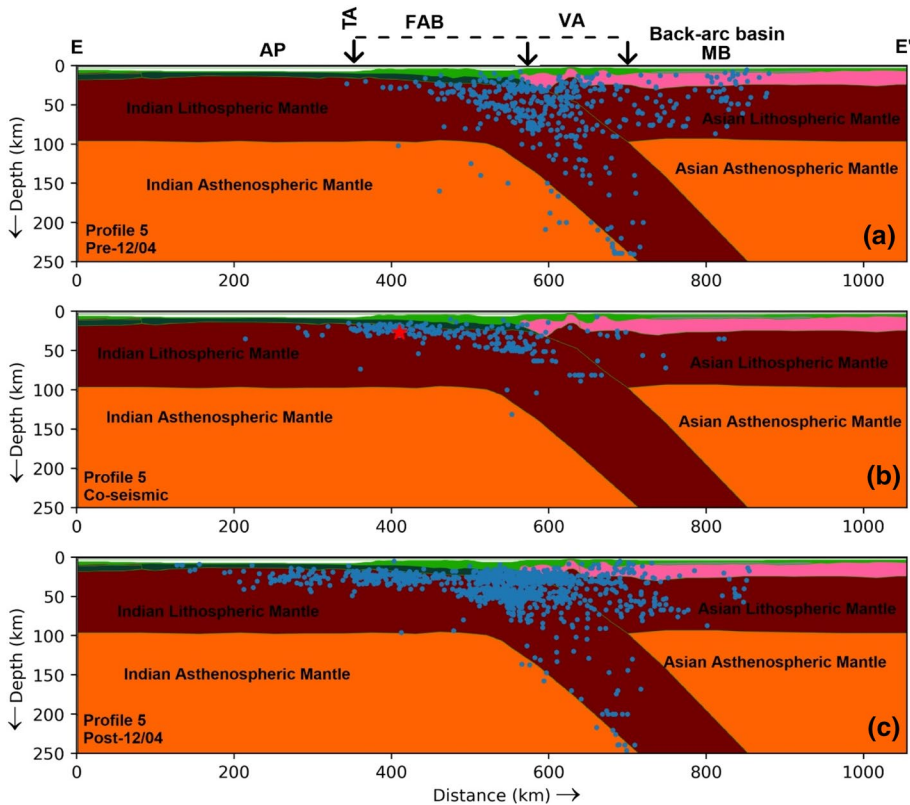


Fig. 15 Depth sections showing the distributions of earthquakes in different tectonic units along profile 5 of sector 1 under pre- (a), co- (b) and post-seismic (c) deformation phases

converging plates (Khan et al. 2017, 2018) also support these observations. Although the seismic activities under post-12/04 phase are quite significant and follow the pattern of pre-12/04 phase, an additional band of activities is found near the trench axis (Fig. 10c). It is also found that the area adjacent to NER became more active during this phase.

The hypocenter projection on gravity profiles shows mainly two distinct clusters of seismicity under pre-seismic deformation phase (pre-12/04): the first cluster is associated with the sharp bending zone of the subducting lithosphere, while the second cluster is observed on the overriding plate, predominantly associated with the back-arc region (Figs. 11, 12, 13, 14, 15). However, ocean-ward migration of the concentration of seismicity is observed along profiles 4 and 5 in sectors 4 and 5; little distinct separation of seismicity is apparent for both the lithosphere in sector 5 (Figs. 14a, 15a). A seismic-patch between $\sim 6^\circ$ and 14° N on the overriding plate accounts for extension of the active volcanic arc. During the post deformation phase (post-12/04), an apparent migration of intraplate seismicity is found toward the shallower part of the oceanic lithosphere, while more intense deformation is found toward oceanic part in sector 5 (Fig. 15c) and complies with the geodetic observations (Subarya et al. 2006; Prawirodirdjo et al. 2010). A wide zone of deformation is found in the underriding plate in sector 5 (Fig. 15b) under co-seismic phase. The lateral extension of this deformation zone sharply decreases toward north from sectors 4 to 2 (Figs. 12, 13,

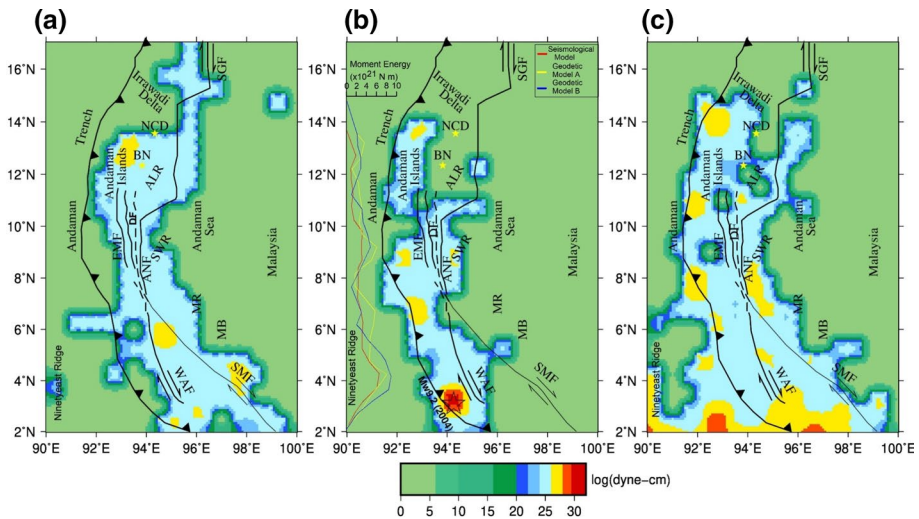


Fig. 16 Maps illustrating the release of seismic moment (dyne-cm) of earthquakes with moment magnitude M_w 4.0 and above under pre- (a), co- (b) and post-seismic (c) deformation phases. Plot in b illustrates the seismic moment release reconstructed based on seismological data and geodetic models (after Subarya et al. 2006). The color index below shows the seismic moment. The abbreviated annotations are explained in the caption of Fig. 1. The lateral shifting of maximum energy toward the trench subsequent to the 2004 mega-event can be seen here

14) and almost dies out further in sector 1 (Fig. 11b) in this phase. The ~ 1500 km rupture of the 2004 mega-event sharply reduced around the north Andaman area (Subarya et al. 2006; Chlieh et al. 2007) and accounts for arc-controlled deformation along the plate margin (Khan et al. 2017).

5.3 Moment Release Characteristics

The release of seismic moment energy under pre-, co- and post-seismic phases relative to the 2004 mega-earthquake was analyzed to understand the deformation processes along the margin (Fig. 16). Under the pre-12/04 phase (Fig. 16a), the higher moment energy values of 10^{24} to 10^{25} dyne-cm were associated with the penetrating lithosphere, paralleling the trench axis, predominantly beneath the fore-arc region. The SGF and SMF, the two transcurrent fault systems, had similar amount of seismic energy in the north and south. Pockets of higher energy of $\sim 10^{27}$ dyne-cm (yellow color patches) are found at few places. In the co-seismic phase (Fig. 16b) (during 12/26/2004 to 12/31/2004), all the earthquakes with magnitude greater than 6 occurred along or near the trench between latitude 6° N and 9° N. Hence, most of the energy releases during this period is found in this region, which is likely to be associated with EMF, DF, ANF, etc. Another high moment energy value is observed to the east of the ALR (96° E, 12° N), which arises due to frequent occurrences of smaller magnitude earthquakes. In the post-12/04 phase (Fig. 16c), the maximum moment energy release is observed along the trench and trench-parallel faults. This energy further died down till the year 2012 except one significant energy release during 2007–08 in the east of Andaman Islands. The other high moment energy releases observed in the southern part of the region were due to two earthquake events with M_w 7.2 and M_w 8.6 in the off

west coast of northern Sumatra in 2012 (Shamim et al. 2019). Similar to co-seismic phase (Fig. 16b), pockets of higher energy were found at 2°–3° N, 7°–8° N, and at around 11° N and 14° N in the post-seismic phase (Fig. 16c). Moment energy plot (Fig. 16b), reconstructed from the seismological and geodetic data (Fig. 4 of Subarya et al. 2006; Lorito et al. 2010), also supports these observations.

6 Discussion

6.1 Structure of the Lithosphere

The five profiles selected at specific locations, orthogonal to the trench axis, apparently resemble E-class subduction zone (Harabaglia and Doglioni 1998), where an intermediate asymmetric shaped negative free-air gravity anomaly is identified around the trench axis. Although the gravity values along the profiles (Figs. 5, 6, 7, 8, 9) show broadly similar patterns comparable to those of a typical subduction margin, each gravity profile is unique in structure. For example, all the profiles show prominent negative gravity anomaly and thick fore-arc basin with sedimentary layer and TRC. The AP area documents little positive gravity values along the profiles 1–4. On the other hand, the VA documents positive gravity anomaly with variable lateral extension. Although the lateral extension of the FAB along all the profiles varies partially, an increased extension is noted in profiles 2, 3 and 5. These differences are suggested to be caused by the change of the curvature of the arc system and the rate of subduction, with concomitant increase in the dip of the subducting lithosphere from south to north beneath the overriding Asian plate (Khan and Chakraborty 2005; Carter and Bandopadhyay 2017a, b). The transitional crusts and the Moho in most of the sectors record moderate to intense deformation that might be caused by eastward penetration of the Indian oceanic lithosphere beneath the Asian plate. Such deformation is marked by the frequent changes in geometry of the Moho all along the profiles (cf. Figs. 5, 6, 7, 8, 9). A sharp change of depth of Moho is found around the Andaman Sea spreading center along profile 2 (Fig. 6), whereas small change in Moho depths is found in other sectors. The NER is delineated only along profiles 4 and 5, but is not found along profile 3 at about 10° N latitude. Beyond 10° N the NER possibly forms a buried anticlinal uplift of the oceanic basement under the sediments and cannot be distinguished from the subduction zone here (Curry et al. 1982; Gopala Rao et al. 1997; Krishna et al. 1999; Subrahmanyam et al. 2008; Levchenko et al. 2010; Michael and Krishna 2011). The NER, further toward north, changes its trend toward northeast; converges on the Andaman fore-arc (Franke et al. 2008; Subrahmanyam et al. 2008; Kumar et al. 2013); and apparently forms a tri-junction with the Andaman trench and the Sumatra trench (Socquet et al. 2006). The oceanic crust and the Moho in sector 5 have suffered an intense deformation beneath the AP as well as the overriding plate (Fig. 9), and presumably record strong convergence of both the plates and enhanced coupling along the interplate region. A quite thin sediment layer is identified between 4° and 10° N, the area of increased interaction between NER and the trench.

The structural/tectonic elements of the subduction margin were identified from the overall topographic variations, the pattern of gravity anomaly, thicknesses of different layers of the lithosphere in the plates involved, geometry of the plates and positions of different tectonic units with respect to the different structural/tectonic features. The presence of the outer swell (outer bathymetric high) on the AP of the Indo-Australian plate is identified from its continuity from the north to south defined by a slight positive (~40 mGal) gravity

anomaly toward the western side of the Andaman Trench (Fig. 2). The position of the trench is marked by a low negative (~ -40 mGal) gravity anomaly. This low value results from thick sedimentary layer as well as deeper position of Moho because of downward bending of the slabs, resulting in the lowest value (~ -200 mGal) below the tectonic accretionary prism. This zone of minimum gravity value extends more or less continuously, parallel to the trench axis, at an average distance of ~ 150 km (Fig. 2). The zone of positive gravity anomaly between the two gravity low zones represents the outer part of the FAB (the sedimentary ridge) which has crustal accretions on the overriding plate (the tectonic accretionary prism). Scrapping of parts of the subducting oceanic crust and their addition to the overlying block by the thrusts results in the observed positive gravity pattern. The VA shows high positive gravity anomaly and is identified toward the east of the FAB gravity low zone. Though the VA can be easily identified at the southern end near Sumatra, the identity of the VA in the central and northern part becomes subdued mainly because of the presence of transtensional deformation. The presence of a series of N–S striking dextral strike-slip faults and NE–SW striking extensional basins (developing spreading ridges) dissect the VA and inhibit its full development (cf. EMF, DF, ANF, WAF, ALR, SWR and MR in Figs. 1, 2).

The profile 1 on the northern part of the area shows the topographic and gravity anomaly patterns typical of an island-arc-type subduction margin, with well-developed trench, FAB, VA and BAB (Fig. 5). The VA is marked by the presence of active volcanoes at NCD. The thickened TR below the FAB of the overriding plate due to crustal accretion is the possible reason for increased gravity value below FAB, compared to the minimum of ~ -200 mGal in other sectors. The profile 2 (Fig. 6) has similar structural features as in profile 1, but this profile shows a zone of low positive gravity high between the two gravity low zones of the trench and the FAB. As discussed earlier this high has developed due to the presence of thin slices of the off-scraped oceanic crust transported by thrusts sympathetic to the plate boundary. A very thick sedimentary layer in profile 2 (Fig. 6) represents this tectonic accretionary prism. The VA is represented by the Barren island volcanic center located to the east of the gravity low of ~ -120 mGal. However, the topography as well as the gravity anomaly over the VA has subdued pattern due to the interaction of the ENE–WSW trending ALK ridge. It may be noted that the boundary of Sectors 2 and 3 is located over the Andaman sea spreading center (ASC), separating ALK and SWR. Therefore, we infer that relatively high heat flow of the ALK ridge may be the reason for an overall lower density of rocks in the VA and the resultant subdued gravity anomaly. The profile 3 (Fig. 7) shows patterns similar to the profile 2. In this profile, the ASC intersects the profile line to the west of the VA, resulting in the development of a prominent topographic low (pull-apart basin) to the west of the VA. A wide FAB with a very thick tectonic accretionary prism is the other main tectonic feature along this profile. The profile 4 (Fig. 8) also shows tectonic features similar to those in Sectors 2 and 3, but presence of the NER on the AP of the subducting plate is an additional feature along this profile. The width of the FAB has been reduced little in this profile. Further, the curvature of the trench has a significant change near this profile (compared to the convex side toward the subducting plate on the west, this zone has a concave side toward the west), and the tectonic accretionary prism has maximum thickness, but the positive gravity anomaly visible in other profiles is missing (subdued). We interpret these features to be the result of (a) the interaction of the NER, causing the plate boundary to become deformed and curved up (antiformal geometry) giving rise to eastward curvature (westward concavity), and (b) interaction of the southwestern part of the SWR and deeper Moho of the overlying plate resulting in overall low gravity value. Overall patterns of this profile are similar to those in profile 1. The profile 5 (Fig. 9) shows

the crustal structures of the NER on the west, the trench, the sliver plate, a narrow pull-apart basin associated with the WAF passing through the FAB, the well-developed VA on the northwestern part of the Sumatra Island and the back-arc basin (MB). The tectonic features are similar to those observed in the profile 2. Substantial differences in the tectonic patterns between profile 5 and profile 4 indicate that the boundary between the Sectors 5 and 4 is a zone of significant changes in structural features due to the interactions between the NER on the west and different spreading centers in the east (MR and SWR). This zone of interaction possibly represents strong interaction between both the plates generating maximum energy for seismicity.

6.2 Seismic Deformation of the Lithosphere

Projections of hypocenters on the five gravity models illustrate the concentration of seismicity relative to different tectonic elements identified along the profiles (Figs. 11, 12, 13, 14, 15). It is apparent from all five profiles and seismicity map (Fig. 10a) that prior to the 2004 mega-event (i.e., pre-12/04 phase), seismic activities were virtually absent near the trench toward west. These were mainly distributed within the inclined Benioff zone as well as in the overriding lithosphere, particularly beneath the back-arc region (Figs. 10a, 11, 12, 13, 14, 15). Although the seismicity in the co-seismic deformation phase was confined to the flexing zones of the lithosphere, with little distribution in the overriding plate (Fig. 10b), the lateral extent of the zone of intraplate deformation was wider and might have been caused by increased seismic coupling toward south (Figs. 10b, 15c) (Khan et al. 2020). Very wide similar intraplate deformation was also found in sector 5 under post-12/04 phase (Fig. 15c). Thus, the wide deformation phase is invariably recorded in sector 5 for all the phases (Figs. 10b, 15c), which accounts for intense seismic coupling between the converging plates in this area.

The decreasing lateral extent of the distribution of intraplate seismicity toward north accounts for reduction of seismic coupling, which becomes maximum in sector 1 (Figs. 10, 11, 12, 13, 14, 15). The evolution and deformation of this margin are linked with the Late Cenozoic convergence of the Indian and Asian plates (Rodolfo 1969; Karig et al. 1980; Le Dain et al. 1984; Peltzer and Tapponnier 1988; McCaffrey 1991; Hall 1997; Curray 2005; Khan 2005; Khan and Chakraborty 2005). The opening and migration of the Andaman Sea spreading centre (Khan and Chakraborty 2005), incidents of great-to-mega-earthquakes (Khan et al. 2018) and critical obliquity of the converging Indian plate (McCaffrey et al. 2000) were identified in sector 5. Tearing of mantle penetrating lithosphere and the sharp change in length of the dipping lithosphere from Java to Sumatra (Shamim et al. 2019 and references therein) and the minimum plate flexing depth and dip near the NW Sumatra clearly support this observation. Significant numbers of earthquakes have also been identified beneath the MR (cf. Figs. 10, 15).

We further observe that the seismic activities invariably migrated toward the trench from the source region of the 2004 mega-event. It is also important to note that the events migrated toward the subducting oceanic plate and passed the TA in the south (Fig. 11), but terminated almost near the TA in the north (Fig. 11). This might have been caused by dominant extension in the Andaman–Sea back-arc area. Here, large amount of seismic energy was released in the form of earthquakes under both pre-12/04 and post-12/04 deformation phases (Fig. 11, Khan et al. 2017). Engdahl et al. (2007), Mishra et al (2007a, b), and Andrade and Rajendran (2014) also observed a shift of aftershock activities from deep to shallow level of the lithosphere. Hsu et al. (2006) and Lubis et al. (2013) also reported

the shifting of aftershocks from deep to shallow part of the subducting oceanic lithosphere following the 2005 M_w 8.7 Nias earthquake, and this was supported by the GPS observations (Subarya et al. 2006; Prawirodirdjo et al. 2010).

Similar shifts of aftershocks were also identified by Ammon et al. (2008) and Lay et al. (2009) along the Kurile trench following the incident of November 15, 2006, M_w 8.3 earthquake. This was interpreted to be caused by stress transfer through the subducting lithosphere, which later triggered the 2007 M_w 8.1 normal faulting event in the outer-rise area. Intensification of extensional stresses enabled by the reduction of compressional stress in the lower part of the subducting plate possibly caused such deformation at the shallower part of the slab (Chapple and Forsyth 1979). Christensen and Ruff (1988) proposed the role of variations of interplate coupling and presence of tensional stress related earthquakes due to bending of the subducting plate and the slab-pull force. Some activities were also recorded along the NER. Clustered seismic activity around the ASR after the 2004 mega-event was possibly caused by volcanic eruption or reactivation of the back-arc (Bandopadhyay et al. 2006; Laluraj et al. 2006; Bandopadhyay 2017). The decrease in concentration of seismicity from south to north is also well corroborated with the observation of increasing obliquity of the converging Indian lithosphere toward the north (Khan and Chakraborty 2005).

6.3 Seismic Energy Release Characteristics and the Margin Tectonics

Figure 16a illustrates the characteristics of seismic moment energy release during pre-12/04 phase. We observe a low- to moderate-energy band paralleling the trench axis. Three main patches of moderate energy release, apparently noted at arbitrary locations, might be correlated with segment-specific tectonics along the margin (Prawirodirdjo et al. 2010). The discontinuous patches of moderate energy release, located close to the trench axis under both co- and post-12/04 phases (Fig. 16b, c), possibly indicate enhanced deformation at the shallower segment of the subducting Indian lithosphere and/or variations of physical properties of the interplate region. Ocean Bottom Seismometer studies by Lin et al. (2009) for the aftershocks of 2004 in the month of July 2005 recorded two different patterns of seismic activities along two separate splay faults, paralleling the Sumatra trench axis. They found sharp drop of seismicity beyond 5.7° N toward north and correlated with the change in physical properties of the slab interface of the region. Khan (2007), Khan et al. (2012, 2017) found a correlation between (i) the moment energy releases and rupture speed of the 2004 mega-event, (ii) variations of aftershock concentration with dip of the subducting lithosphere vis-à-vis plate driving forces and (iii) plate obliquity along the Andaman–Nicobar–Sumatra margin.

The M_w 7.5 2009 event beneath the trench near 8° N (Fig. 1) is correlated with the arc-controlled tectonics where the second energy burst of the 2004 event took place near the Car Nicobar area 300 s later after the main shock (Fig. 3 of Ishii et al. 2005 and Fig. 16b). Occurrence of another M_w 7.5 event in 2009 (Fig. 1) complies with the moderate energy release near 14° N (Fig. 12c) and is interpreted to be caused by interaction of the NER against the Andaman trench. The present observation of seismicity distribution and moment energy release comply with the segment-specific energy burst with inhomogeneous slip distribution (Ishii et al. 2005; Ammon et al. 2005; Subarya et al. 2006; Chlieh et al. 2007; Lorito et al. 2010), and segmented-specific thrust movements (Prawirodirdjo et al. 2010) along the margin during 2004 mega-event. The maximum energy release areas (yellow color band) coincide with two M_w 7.2 events in 2010, and one each of M_w 7.8 in

2010, M_w 8.6 in 2012, and M_w 7.2 in 2012 (Fig. 1). The coincidence of maximum coupling between the two plates along this margin (Scholz and Campos 1995; Prawirodirdjo et al. 1997) and the minimum flexing depth of the Indian lithosphere to the northwest of Sumatra (Khan and Chakraborty 2005) are interpreted to be the causative factors for the release of maximum seismic energy (cf. Fig. 12b) as well as concentration of high seismicity near the area around 3° N; 95.5° E (cf. Fig. 11).

7 Conclusions

Spectral analysis of gravity data combined with the gravity modeling of the Andaman–Nicobar–Sumatra subduction margin led to demarcation of different tectonic units of the region. The presence of the outer swell (outer bathymetric high), the trench, tectonic accretionary prism, the fore-arc basin, the volcanic arc, the pull-apart (transtensional) basins and the back-arc basin have been well demarcated in the maps and profiles. Distribution of seismicity and moment release characteristics related to different temporal domains of the 2004 M_w 9.2 earthquake were analyzed in their tectonic context. The minimum gravity anomaly (~ -200 to -120 mGal), parallel to the trench axis along the fore-arc shear fault on the eastern boundary of the sliver plate, is found to be associated with a sharp bend of the descending Indian lithosphere (cf. McCaffrey 1991; Liu et al. 1995). The preferential incidents of earthquakes around the sharp bend of the subducting lithosphere, showing moderate energy release in pre-12/04 phase (Figs. 11, 12, 13, 14, 15), are correlated with long-term deformation, and seismogenic behavior along the subduction margin (cf. Song and Simons 2003; Wells et al. 2003; Khan et al. 2012). Previous work along subduction margins also found that the subducting lithosphere could sustain a maximum bending stress of an order of magnitude higher than the maximum strength of the oceanic lithosphere (cf. Kohlstedt et al. 1995; Conrad and Hager 1999).

A high gravity anomaly between the Sumatra trench and the NER is interpreted to be associated with high-density mantle materials present at a shallow level. Moderately positive (> 10 mGal) to high (> 100 mGal) gravity values in the Andaman Sea basin are presumably associated with the shallow mantle materials evolved through spreading of the back-arc during the Late Miocene-Pliocene time (Kamesh Raju et al. 2004; Khan and Chakraborty 2005). Wide negative gravity anomalies in sectors 2 and 3 of the central part coincide with a more deformed accreted fore-arc basin (Singh and Moeremans 2017), apparently located in a zone of increased interaction between the Ninetyeast Ridge and the Andaman trench (Gahalaut et al. 2010; Carter and Bandopadhyay 2017a, b).

The major outcomes of the present work are given below.

- Absence of seismic activity near the trench under pre-12/04 phase (Figs. 10, 11, 12, 13, 14, 15) apparently suggests a long-term quiescence in the area.
- A high concentration of the seismicity in the back-arc area of the central segment (Figs. 13, 14) and distributed nature of seismicity over a wide zone in the southern segment (i.e., sector 5, Fig. 15) are noted under both pre- and post-12/04 phases (Fig. 10a, c).
- A shift of seismic activities toward the trench from pre-12/04 to post-12/04 phases occurred in sectors 4 and 5 (Figs. 14, 15).

- Lateral segmentation of the seismic energy band (yellow patches in Fig. 16) was caused by active deformation, and migration of seismic activity from upper-most part to the shallower part of the subducting Indian lithosphere.
- A dominant extension in the back-arc, the Andaman Sea spreading centre in the northern part, restricted the shifting of aftershocks as well as release of seismic energy up to the trench, while the absence of extensional tectonic domain in the south allowed seismic shocks to migrate westward beyond the trench.
- The intense seismic activities under both pre-12/04 and post-12/04 seismic phases were found to be associated with the back-arc area, where several faults (EMF, DF and ANF) became active after the 2004 mega-event (Figs. 11, 12, 13, 14, 15).
- Many great earthquakes ($M_w > 7.0$) near the trench toward south indicate active deformation of the lithosphere near the 2004 mega-events (Fig. 1; this deformation is illustrated by yellow and red patches in the area (Fig. 16c)). The seismic activity was quite intense in the area between the NER and the Sumatra trench (Fig. 10c)
- Two earthquakes of magnitude 7.5 (M_w) in 2009 near 8° N and 14° N latitudes, close to the trench axis, indicate significant deformation of the subducting lithosphere (Fig. 1).
- Well-correlated energy bursts identified on seismological and geodetic models (Fig. 16b) provide support for seismic segmentation of the entire Andaman–Nicobar–Sumatra margin.
- Decrease in moment release northward from northwest Sumatra during the 2004 and 2005 events (Fig. 16c) was caused by its increased plate convergence obliquity between the Indo-Australian and the Eurasian plates and was one of the major factors for enhanced accommodation and pre-, co- and post-seismic moment release in the Andaman–Sumatra area.
- Wide lateral extension of seismicity distribution was maximum in sector 5 and decreased toward north to have a minimum value in sector 1 (Figs. 11, 12, 13, 14, 15).
- The seismic coupling between the underriding and overriding plates is interpreted to be maximum in the southern part (sector 5) of the study area.
- The flexing zone of the subducting Indian oceanic lithosphere was recorded as the nodal area of strain energy accumulation along the entire margin.

Acknowledgements The study was supported by the Department of Science and Technology, Government of India, New Delhi. The authors are thankful to Lisa C. McNeill and Natasha Bushenkova for their review comments and suggestions, which has improved the manuscript greatly. The authors are also grateful to O.B. Andersen for sharing the DTU15 model gravity data.

References

- Ammon CJ, Ji C, Theo HK, Robinson D, Ni S, Hjorleifsdottir V, Kanamori H, Lay T, Das S, Helmberger D, Ichinore G, Polet J, Wald D (2005) Rupture process of the 2004 Sumatra–Andaman earthquake. *Science* 308:1133–1139
- Ammon CJ, Kanamori H, Lay T (2008) A great earthquake doublet and seismic stress transfer cycle in the central Kuril islands. *Nature* 451:561–566
- Andersen OB, Stenseng L, Piccioni G, Knudsen P (2016) The DTU15 MSS (mean sea surface) and DTU-15LAT (lowest astronomical tide) reference surface. In: ESA Living Planet symposium 2016
- Andrade V, Rajendran K (2014) The April 2012 Indian Ocean earthquakes: seismotectonic context and implications for their mechanisms. *Tectonophysics* 617:126–139
- Bandopadhyay PC (2017) Inner-arc volcanism: Barren and Narcondam islands. *Geol Soc Lond Mem* 47:167–192. <https://doi.org/10.1144/M47.12>

- Bandopadhyay PC, Carter A (2017) Geological framework of the Andaman–Nicobar Islands. *Geol Soc Lond Mem* 47:75–93. <https://doi.org/10.1144/M47.6>
- Bandopadhyay PC, Sumit KM, Pal T (2006) The 2005 eruption on Barren Island, Andaman Sea. *Curr Sci* 90(5):620–622
- Bansal AR, Dimri VP (2010) Scaling spectral analysis: a new tool for analysis for interpretation of gravity and magnetic data. *E-J Earth Sci India* 3(1):54–68
- Bennett SEK, Oskin ME, Iriondot A, Kunk MJ (2016) Slip history of the La Cruz fault: development of a late Miocene transform in response to increased rift obliquity in the northern Gulf of California. *Tectonophysics* 693:409–435
- Bevis M, Taylor FW, Schutz BE, Recy J, Isaks BL, Helu S, Singh R, Kendrick E, Stowell J, Taylor B, Calmant B (1995) Geodetic observations of very rapid convergence and back-arc extension at the Tonga Arc. *Nature* 374:249–251
- Bilham R (2005) A flying start, then a slow slip. *Science* 308:1126–1127
- Bletery Q, Sladen A, Jiang J, Simons MA (2016) Bayesian source model for the 2004 great Sumatra–Andaman earthquake. *J Geophys Res* 121(7):5116–5135
- Brune S (2014) Evolution of stress and fault patterns in oblique rift systems: 3-D numerical lithospheric-scale experiments from rift to breakup. *Geochem Geophys Geosyst* 15:3392–3415
- Cao A, Gao SS (2002) Temporal variation of seismic *b*-values beneath north-eastern Japan island arc. *Geophys Res Lett* 29(48):1–3
- Cardwell RK, Isacks BL (1978) Geometry of the subducted lithosphere beneath the Banda Sea in eastern Indonesia from seismicity and fault plane solutions. *J Geophys Res* 83:2825–2838
- Carter A, Bandopadhyay PC (2017a) Seismicity of the Andaman–Nicobar Islands and Andaman Sea. *Geol Soc Lond Mem* 47:205–213. <https://doi.org/10.1144/M47.14>
- Carter A, Bandopadhyay PC (2017b) The 26 December 2004 earthquake and tsunami. *Geol Soc Lond Mem* 47:215–224. <https://doi.org/10.1144/M47.15>
- Castelltort S, Goren L, Willett SD, Champagnac L, Herman F, Braun L (2012) River drainage patterns in the New Zealand Alps primarily controlled by plate tectonic strain. *Nat Geosci* 5:744–748
- Catherine JK, Gahalaut VK, Sahu VK (2005) Constraints on rupture of the December 26, 2004, Sumatra earthquake from far-field GPS observations. *Earth Planet Sci Lett* 237(3):673–679
- Chakraborty PP, Khan PK (2009) Cenozoic geodynamic evolution of the Andaman–Sumatra subduction margin: a current understanding. *Island Arc* 18:184–200
- Chamoli A, Dimri VP (2010) Spectral analysis of gravity data of NW Himalaya. In: International workshop adding new value to electromagnetic, gravity and magnetic methods for exploration Capri, Italy. EGM 2010. http://www.eageseg.org/data/egm2010/Sessione%20C/Oral%20papers/C_OP_23.pdf
- Chapple WM, Forsyth DW (1979) Earthquakes and bending of plates at trenches. *J Geophys Res* 84:6729–6749
- Charusiri P, Imsamut S, Zhuang Z, Ampaiwan T, Xu X (2006) Paleomagnetism of the earliest Cretaceous to early late Cretaceous sandstones, Khorat Group, Northeast Thailand: implications for tectonic plate movement of the Indochina block. *Gondwana Res* 9:310–325
- Chemenda A, Lallemand S, Bokun A (2000) Strain partitioning and interplate friction in oblique subduction zones: constraints provided by experimental modeling. *J Geophys Res* 105:5567–5581
- Chlieh M, Avouac JP, Hjorleifsdottir V, Song TRA, Ji C, Sieh K, Sladen A, Hebert H, Prawirodirdjo L, Bock Y, Galetzka J (2007) Coseismic slip and afterslip of the Great M_w 9.15 Sumatra–Andaman Earthquake of 2004. *Bull Seismol Soc Am* 97(1A):S152–S173
- Christensen DH, Ruff LJ (1988) Seismic coupling and outer rise earthquakes. *J Geophys Res* 93:13421–13444
- Christova C (2004) Stress field in the Ryukyu–Kyushu Wadati–Benioff zone by inversion of earthquake focal mechanisms. *Tectonophysics* 384:175–189
- Clift PD (2017) Regional context of the geology of the Andaman–Nicobar accretionary ridge. *Geol Soc Lond Mem* 47:19–26. <https://doi.org/10.1144/M47.3>
- Cloos M (1992) Thrust-type subduction-zone earthquakes and seamount asperities: a physical model for seismic rupture. *Geology* 20:601–604
- Conrad CP, Hager BH (1999) Effects of plate bending and fault strength at subduction zones on plate dynamics. *J Geophys Res* 104:17551–17571
- Conrad CP, Bilek S, Lithgow-Bertelloni C (2004) Great earthquakes and slab pull: interaction between seismic coupling and plate-slab coupling. *Earth Planet Sci Lett* 218:109–122
- Curry JR (2005) Tectonics and history of the Andaman Sea region. *J Asian Earth Sci* 25:187–232
- Curry JR, Munasinghe T (1991) Origin of the Rajmahal traps and the 85_E Ridge: preliminary reconstructions of the trace of the Crozet Hotspot. *Geology* 19:1237–1240

- Curry JR, Moore DG, Lawyer LA (1979) Tectonics of the Andaman sea and Burma. In: Watkins JS (ed) Geological and geophysical investigations of continent margins. American Association of Petroleum Geologists, Memoir 29:189–198
- Curry JR, Emmel FJ, Moore DG, Russel WR (1982) Structure, tectonics, and geological history of the northeastern Indian Ocean. In: Nairn AE, Stehli FG (eds) The Ocean Basins and Margins, The Indian Ocean, vol 6. Plenum, New York, pp 399–450
- Dasgupta S, Mukhopadhyay M, Bhattacharya A, Jana TK (2003) The geometry of the Burma–Andaman subducting lithosphere. *J Seismol* 7:155–174
- DeMets C, Gordon RG, Argus DF, Stein D (1994) Effect of recent revisions to the geomagnetic reversal time scale and estimates of current plate motions. *Geophys Res Lett* 21:2191–2194
- Dessa JX, Klingelhoefer F, Graindorge D, André C, Permana H, Gutscher MA, Chauhan A, Singh SC, the SUMATRA-OBS Scientific Team (2009) Megathrust earthquakes can nucleate in the forearc mantle: evidence from the 2004 Sumatra event. *Geology* 37:659–662
- Dewey JW, Choy G, Presgrave B, Sipkin S, Tarr AC, Benz H, Earle P, Wald D (2007) Seismicity associated with the Sumatra–Andaman Islands earthquake of 26 December 2004. *Bull Seismol Soc Am* 97:25–42
- Diamant M, Harjono H, Karta K, Deplus C, Dahrin D, Zen MT Jr, Gerard M, Lassal O, Martin A, Malod JA (1992) Mentawai fault zone off Sumatra: a new key to the geodynamics of western Indonesia. *Geology* 20:259–262
- Divins DL (2003) Total sediment thickness of the world's oceans and marginal seas. NOAA National Geophysical Data Center, Boulder
- Dziewonski AM, Anderson DL (1981) Preliminary reference Earth model. *Phys Earth Planet Inter* 25(4):297–356
- Earnest A, Rajendran CP, Rajendran K, Anu R, Arun GM (2005) Near-field observations on the co-seismic deformation associated with the 26 December 2004 Andaman–Sumatra earthquake. *Curr Sci* 89:1237–1244
- Engdahl ER, Villaseñor A (2002) Global seismicity: 1990–1999. In: Lee WHK, Kanamori H, Jennings PC, Kisslinger C (eds) International handbook of earthquake and engineering seismology, part A (Chapter 41). Academic Press, New York, pp 665–690
- Engdahl ER, van der Hilst R, Buland R (1998) Global teleseismic earthquake relocation with improved travel times and procedures for depth determination. *Bull Seismol Soc Am* 88:722–743
- Engdahl ER, Villaseñor A, DeShon HR, Thurber CH (2007) Teleseismic relocation and assessment of seismicity (1918–2005) in the region of the 2004 M_w 9.0 Sumatra–Andaman and 2005 M_w 8.6 Nias Island great earthquakes. *Bull Seismol Soc Am* 97:S43–S61
- Fitch TJ (1972) Plate convergence, transcurent faults and internal deformation adjacent to Southeast Asia and western Pacific. *J Geophys Res* 77:4432–4460
- Fowler CMR (2009) The solid Earth: an introduction to global geophysics. Cambridge University Press, Cambridge, U.K., p 685
- Franke DS, Schnabel M, Ladage S, David T, Neben S, Djajadihardja YS, Muller C, Kopp H, Gaedicke C (2008) The great Sumatra–Andaman earthquakes—imaging the boundary between the ruptures of the great 2004 and 2005 earthquakes. *Earth Planet Sci Lett* 269:118–130
- Furlong KP, Chapman DS, Alfred PW (1982) Thermal modeling of the geometry of subduction with implications for the tectonics of the overriding plate. *J Geophys Res* 87:1786–1802
- Gahalaut VK, Nagarajan B, Catherine JK, Kumar S (2006) Constraints on 2004 Sumatra–Andaman earthquake rupture from GPS measurements in Andaman–Nicobar Islands. *Earth Planet Sci Lett* 242:365–374
- Gahalaut VK, Subrahmanyam C, Kundu B, Catherine JK, Ambikapathy A (2010) Slow rupture in Andaman during 2004 Sumatra–Andaman earthquake: a probable consequence of subduction of 90° E ridge. *Geophys J Int* 180:1181–1186
- Ghosh GK, Singh CL (2014) Spectral analysis and Euler deconvolution technique of gravity data to decipher the basement depth in the Dehradun–Badrinath area. *J Geol Soc India* 83(5):501–512
- Gopala Rao D, Krishna KS, Sar D (1997) Crustal evolution and sedimentation history of the Bay of Bengal since the Cretaceous. *J Geophys Res* 102:17747–17768
- Gordon RG, DeMets C, Royer JY (1998) Evidence for long-term diffuse deformation of the lithosphere of the equatorial Indian Ocean. *Nature* 395:370–374
- Gudmundsson Ó, Sambridge M (1998) A regionalized upper mantle (RUM) seismic model. *J Geophys Res* 103:7121–7136
- Guerit L, Dominguez S, Malavieille J, Castelltort S (2016) Deformation of an experimental drainage network in oblique collision. *Tectonophysics* 693:210–222

- Hahn A, Kind EG, Mishra DC (1976) Depth estimation of magnetic sources by means of Fourier amplitude spectra. *Geophys Prospect* 24:287–308
- Hall R (1996) Reconstruction Cenozoic SE Asia. In: Hall R, Blundell DJ (eds) *Tectonic evolution of SE Asia*. Geological Society, Special Publications 106:153–184
- Hall R (1997) Cenozoic plate tectonic reconstructions of SE Asia. Geological Society, London, Special Publications 126(1):11–23
- Hall R (2002) Cenozoic geological and plate tectonic evolution of SE Asia and the SW Pacific: computer-based reconstructions and animations. *J Asian Earth Sci* 20:353–434
- Harabaglia P, Doglioni C (1998) Topography and gravity across subduction zones. *Geophys Res Lett* 25(5):703–706
- Henstock TJ, McNeill LC, Bull JM, Cook BJ, Gulick SP, Austin JA, Permana H, Djajadihardja YS (2016) Downgoing plate topography stopped rupture in the A.D. 2005 Sumatra earthquake. *Geology* 44(1):71–74
- Henstock TJ, McNeill LC, Bull JM, Cook BJ, Gulick SPS, Austin JA, Permana JH, Djajadihardja YS (2017) Downgoing plate topography stopped rupture in the A.D. 2005 Sumatra earthquake. *Geology* 44:71–74
- Hecceg M, Artemieva IM, Thybo H (2016) Sensitivity analysis of crustal correction for calculation of lithospheric mantle density from gravity data. *Geophys J Int* 204:687–696
- Heuret A, Lallemand S (2005) Plate motions, slab dynamics and back-arc deformation. *Phys Earth Planet Inter* 1491–1492:31–51
- Heuret A, Funicello F, Faccenna C, Lallemand S (2007) Plate kinematics, slab shape and back-arc stress: a comparison between laboratory models and current subduction zones. *Earth Planet Sci Lett* 256:473–483
- Hsu YJ, Simons M, Avouac J-P, Galetzka J, Sieh K, Chlieh M, Natawidjaja D, Prawirodirdjo L, Bock Y (2006) Frictional afterslip following the M_w 8.7, 2005 Nias–Simeulue earthquake, Sumatra. *Science* 312:1921–1926
- Indriana RD (2008) Estimasi ketebalan sedimen dan kedalaman diskontinuitas Mohorovicic daerah Jawa Timur dengan analisis power spectrum dan data anomlai gravitasi. *Berkala Fisika* 11(2):67–74
- Ishii M, Shearer P, Houston H, Vidale JE (2005) Extent, duration and speed of the 2004 Sumatra–Andaman earthquake imaged by the hi-net array. *Nature* 435:933–936
- Jacob J, Dyment J, Yatheesh V (2014) Revisiting the structure, age, and evolution of the Wharton Basin to better understand subduction under Indonesia. *J Geophys Res* 119:169–190. <https://doi.org/10.1002/2013JB010285>
- Jade S, Ananda MB, Kumar PD, Banerjee S (2005) Co-seismic and post-seismic displacements in Andaman and Nicobar Islands from GPS measurements. *Curr Sci* 88:1980–1984
- Kamesh Raju KA, Ramprasad T, Rao PS, Rao BR, Varghese J (2004) New insights into the tectonic evolution of the Andaman basin, northeast Indian Ocean. *Earth Planet Sci Lett* 221:145–162
- Kamesh Raju KA, Ray D, Mudholkar A, Murty GPS, Gahalaut VK, Samudrala K, Paropkari AL, Ramachandran R, Prakash LS (2012) Tectonic and volcanic implications of a cratered seamount off Nicobar Island, Andaman Sea. *J Asian Earth Sci* 56:42–53
- Kanamori H (1977) The energy release in great earthquakes. *J Geophys Res* 82(20):2981–2987
- Karig DE, Moore GF, Curray JR, Lawrence MB (1980) Morphology and shallow structure of the lower trench slope off Nias Island, Sunda Arc. In: Hayes DE (ed) *The tectonic and geologic evolution of Southeast Asian seas and islands*. American Geophysical Union, Washington, DC, *Geophysical Monograph* 23:179–208
- Karner GD, Watts AB (1983) Gravity anomalies and flexure of the lithosphere at mountain ranges. *J Geophys Res* 87:2923–2948
- Kennett BLN, Cummins PR (2005) The relationship of the seismic source and subduction zone structure for the 2004 December 26 Sumatra–Andaman earthquake. *Earth Planet Sci Lett* 239:1–8
- Khan PK (2005) Variation in dip-angle of the Indian plate subducting beneath the Burma plate and its tectonic implications. *Geosci Int J* 9:227–234
- Khan PK (2007) Lithospheric deformation under pre- and post-seismic stress fields along the Nicobar–Sumatra subduction margin during 2004 Sumatra mega-event and its tectonic implications. *Gondwana Res* 12:468–475
- Khan P, Chakraborty PP (2005) Two-phase opening of Andaman Sea: a new seismotectonics insight. *Earth Planet Sci Lett* 229:259–271
- Khan PK, Chakraborty PP (2009) Plate geometry, plate rheology, and their relation to shallow-focus mega-thrust seismicity with special reference to 26 December 2004 Sumatra event. *J Asian Earth Sci* 34:480–491

- Khan PK, Chakraborty PP, Tarafder G, Mohanty S (2012) Testing the intraplate origin of mega-earthquakes at subduction margins. *Geosci Front* 3:473–481
- Khan PK, Shamim Sk, Mohanty M, Kumar P, Banerjee J (2017) Myanmar–Andaman–Sumatra subduction margin revisited: insights of arc-specific deformations. *J Earth Sci* 28:683–694
- Khan PK, Banerjee J, Shamim Sk, Mohanty M (2018) Long-term seismic observations along Myanmar–Sunda subduction margin: insights for 2004 $M_w > 9.0$ earthquake. *Int J Earth Sci* 107:2383–2392
- Khan PK, Shamim Sk, Mohanty SP, Aggarwal SK (2020) Change of stress patterns during 2004 M_w 9.3 off-Sumatra mega-event: insights from ridge–trench interaction for plate margin deformation. *Geol J* 55:372–389
- Kimura G (1986) Oblique subduction and collision: fore-arc tectonics of the Kurile Arc. *Geology* 14:404–407
- Kohlstedt DL, Evans B, Mackwell SJ (1995) Strength of the lithosphere: constraints imposed by laboratory experiments. *J Geophys Res* 100:17587–17602
- Krishna KS, Gopala Rao D, SubbaRaju LV, Chaubey AK, Shcherbakov VS, Pilipenko AI, Murthy IVR (1999) Paleocene onspreading-axis hotspot volcanism along the Ninetyeast Ridge: an interaction between the Kerguelen hotspot and the Wharton spreading center. *Proc Indian Acad Sci Earth Planet Sci* 108:255–267
- Kuchay OA, Bushenkova NA, Tataurova AA (2015) Structure of the lithosphere and seismotectonic deformations in contact zone of lithospheric plates in the Sumatra Island region. *Geodyn Tectonophys* 6(1):77–89
- Kumar RTR, Windley BF, Rajesh VJ, Santosh M (2013) Elastic thickness structure of the Andaman subduction zone: implications for convergence of the Ninetyeast Ridge. *J Asian Earth Sci* 78:291–300
- Kumar P, Srijoyanthi G, Kumar MR (2016) Seismic evidence for tearing in the subducting Indian slab beneath the Andaman arc. *Geophys Res Lett* 43:4899–4904
- Laluraj CM, Balachandran KK, Sabu P, Panampunnayil SU (2006) Persistent volcanic signature observed around Barren Island, Andaman Sea, India. *Mar Geophys Res* 27:283–288
- Lay T, Kanamori H, Ammon CJ, Nettles M, Ward SN, Aster RC, Beck SL, Bilek SL, Brudzinski MR, Butler R, DeShon HR, Ekstrom G, Satake K, Sipkin S (2005) The great Sumatra–Andaman earthquake of 26 December 2004. *Science* 308:1127–1133
- Lay T, Kanamori H, Ammon CJ, Hutko AR, Furlong K, Rivera L (2009) The 2006–2007 Kuril Islands great earthquake sequence. *J Geophys Res* 114:B11308
- Le Dain AY, Tapponnier P, Molnar P (1984) Active faulting and tectonics of Burma and surrounding regions. *J Geophys Res* 89:453–472
- Leever KA, Gabrielsen RH, Sokoutis D, Willingshofer L (2011) The effect of convergence angle on the kinematic evolution of strain partitioning in transpressional brittle wedges: insight from analog modeling and high-resolution digital image analysis. *Tectonics* 30(2):2TC013. <https://doi.org/10.1029/2010TC002823>
- Levchenko OV, Sager WW, Frey FA, Pringle MS, Krishna KS, Gopala Rao D, Gauntlett E, Mervine E, Marinova YG, Piotrowski A, Paul CF, Huang S, Eisin AE (2010) New geological-geophysical data on the structure of the Ninetyeast Ridge. *Dokl Earth Sci* 434:1208–1213
- Lin J-Y, Le Pichon X, Rangin C, Sibuet J-C, Maury T (2009) Spatial aftershock distribution of the 26 December 2004 great Sumatra–Andaman earthquake in the northern Sumatra area. *Geochem Geophys Geosyst* 10:Q05006
- Liu X, McNally KC, Shen ZK (1995) Evidence for a role in the downgoing slab in earthquake slip partitioning at oblique subduction zones. *J Geophys Res* 100:15351–15372
- Lorito S, Piatanesi A, Cannelli V, Romano F, Melini D (2010) Kinematics and source zone properties of the 2004 Sumatra–Andaman earthquake and tsunamis: nonlinear joint inversion of tide gauge, satellite altimetry, and GPS data. *J Geophys Res* 115:B02304
- Lubis AM, Hashima A, Sato T (2013) Analysis of afterslip distribution following the 2007 September 12 southern Sumatra earthquake using poroelastic and viscoelastic media. *Geophys J Int* 192:18–37
- Lücke OH, Arroyo IG (2015) Density structure and geometry of the Costa Rican subduction zone from 3D gravity modelling and local earthquake data. *Solid Earth* 6(4):1169–1183
- Maung H (1987) Transcurrent movement in the Myanmar Andaman Sea region. *Geology* 15:911–912
- Maus S, Dimri VP (1995) Potential field power spectrum inversion for scaling geology. *J Geophys Res* 100:12605–12616
- McCaffrey R (1991) Slip vectors and stretching of the Sumatran forearc. *Geology* 19:881–884
- McCaffrey R (1992) Oblique plate convergence, slip vectors, and forearc deformation. *J Geophys Res* 97:8905–8915
- McCaffrey R (1993) On the role of the upper plate in great subduction zone earthquake. *J Geophys Res* 98:11953–11966

- McCaffrey R, Zwick PC, Bock Y, Prawirodirdjo L, Genrich JF, Stevens CW, Puntodewo SSO, Subarya C (2000) Strain partitioning during oblique plate convergence in northern Sumatra: geodetic and seismologic constraints and numerical modeling. *J Geophys Res* 105:28363–28376
- McClay K, Whitehouse P, Dooley T, Richards M (2004) 3D evolution of fold and thrust belts formed by oblique convergence. *Mar Pet Geol* 21:857–877
- McNeill LC, Henstock TJ (2014) Forearc structure and morphology along the Sumatra–Andaman subduction zone. *Tectonics* 33:112–134. <https://doi.org/10.1002/2012TC003264>
- Meltzner AJ, Sieh K, Abrams M, Agnew DC, Hudnut KW, Avouac JP, Natawidjaja DH (2006) Uplift and subsidence associated with the great Aceh–Andaman earthquake of 2004. *J Geophys Res* 111:B09101
- Michael L, Krishna KS (2011) Dating of the 85° E ridge (northeastern Indian Ocean) using marine magnetic anomalies. *Curr Sci* 100:1314–1322
- Mishra OP, Chakraborty GK, Singh OP, Kayal JR, Ghosh D (2007a) Aftershock investigation in the Andaman–Nicobar Islands: an antidote to public panic. *Seismol Res Lett* 78:591–600
- Mishra OP, Kayal JR, Chakraborty GK, Singh OP, Ghosh D (2007b) Aftershock Investigation in the Andaman–Nicobar Islands of India and its seismotectonic implications. *Bull Seismol Soc Am* 97:S71–S85
- Mishra OP, Zhao D, Ghosh C, Wang Z, Singh OP, Ghosh B, Mukherjee KK, Saha DK, Chakraborty GK, Gaonkar SG (2011) Role of crustal heterogeneity beneath Andaman–Nicobar Islands and its implications for coastal hazard. *Nat Hazards* 57:51–64
- Mitchell AHG (1981) Phanerozoic plate boundaries in mainland SE Asia, the Himalayas and Tibet. *J Geol Soc* 138:109–122
- Moeremans R, Singh SC (2015) Forearc basin deformation in the Andaman–Nicobar segment of the Sumatra–Andaman subduction zone: insight from high-resolution seismic reflection data. *Tectonics* 34:1736–1750
- Moeremans R, Singh SC, McArdle J, Johansen K (2014) Seismic images of structural variations along the deformation front of the Andaman–Sumatra subduction zone: implications for rupture propagation and tsunamigenesis. *Earth Planet Sci Lett* 386:75–85
- Morley CK (2017) Cenozoic rifting, passive margin development and strike-slip faulting in the Andaman Sea: a discussion of established v. new tectonic models. *Geol Soc Lond Mem* 47:27–50. <https://doi.org/10.1144/M47.4>
- Morley CK, Alvey A (2015) Is spreading prolonged, episodic or incipient in the Andaman Sea? Evidence from deepwater sedimentation. *J Asian Earth Sci* 98:446–456
- Morley CK, Searle M (2017) Regional tectonics, structure and evolution of the Andaman–Nicobar Islands from ophiolite formation and obduction to collision and back-arc spreading. *Geol Soc Lond Mem* 47:51–74. <https://doi.org/10.1144/M47.5>
- Mukhopadhyay M (1988) Gravity anomalies and deep structure of the Andaman arc. *Mar Geophys Res* 9:197–210
- Mukhopadhyay M, Dasgupta S (1988) Deep structure and tectonics of the Burmese arc: constraints from earthquake and gravity data. *Tectonophysics* 149:299–322
- Mukhopadhyay M, Krishna MR (1991) Gravity field and deep structure of the Bengal fan and its surrounding continental margins, northeast Indian Ocean. *Tectonophysics* 186:365–386
- Mukhopadhyay M, Krishna MR (1995) Gravity anomalies and deep structure of the Ninetyeast Ridge north of the equator, Eastern Indian Ocean—a hot spot trace model. *Mar Geophys Res* 17:201–216
- Müller RD, Roest WR, Royer JY, Gahagan LM, Sclater JG (1997) Digital isochrones of the world’s ocean floor. *J Geophys Res* 102:3211–3214
- Patriat P, Achache J (1984) India–Eurasia collision chronology has implications for crustal shortening and driving mechanism of plates. *Nature* 311:615–621
- Paul J, Rajendran C, Lowry A, Andrade V, Rajendran K (2012) Andaman postseismic deformation observations: still slipping after all these years? *Bull Seismol Soc Am* 102(1):343–351
- Peltzer G, Tapponnier P (1988) Formation and evolution of strike-slip faults, rifts, and basins during the India–Asia collision: an experimental approach. *J Geophys Res* 93:15085–15117
- Pesicek JD, Thurber CH, Zhang H, DeShon HR, Engdahl ER, Widiyantoro S (2010) Teleseismic double-difference relocation of earthquakes along the Sumatra–Andaman subduction zone using a 3-D model. *J Geophys Res* 115:B10303
- Ponko SC, Peacock SM (1995) Thermal modeling of the southern Alaska subduction zone: insight into the petrology of the subducting slab and overlying mantle wedge. *J Geophys Res* 100:22117–22128
- Prawirodirdjo L, Bock Y, McCaffrey R, Genrich J, Calais E, Stevens CW, Puntodewo SSO, Subarya C, Rais J, Zwick P, Fauzi RM (1997) Geodetic observations of interseismic strain segmentation at the Sumatra subduction zone. *Geophys Res Lett* 24:2601–2604

- Prawirodirdjo L, McCaffrey R, Chadwell CD, Bock Y, Subarya C (2010) Geodetic observations of an earthquake cycle at the Sumatra subduction zone: role of interseismic strain segmentation. *J Geophys Res Solid Earth* 115(B3):B03414
- Radhakrishna M, Lasitha S, Mukhopadhyay M (2008) Seismicity, gravity anomalies and lithospheric structure of the Andaman arc, North-eastern Indian Ocean. *Tectonophysics* 460:248–262
- Rajendran CP, Rajendran K, Anu R, Earnest A, Machado T, Mohan PM, Freymueller J (2007) Crustal deformation and seismic history associated with the 2004 Indian Ocean earthquake: a perspective from the Andaman–Nicobar Islands. *Bull Seismol Soc Am* 97(1A):S174–S191
- Rajendran K, Rajendran CP, Earnest A, Prasad GR, Dutta K, Ray DK, Anu R (2008) Age estimates of coastal terraces in the Andaman and Nicobar Islands and their tectonic implications. *Tectonophysics* 455(1):53–60
- Ramsey LA, Walker RT, Jackson J (2007) Geomorphic constraints on the active tectonics of Southern Taiwan. *Geophys J Int* 170:1357–1372
- Rapp RH (1998) Comparison of altimeter-derived and ship gravity anomalies in the vicinity of the Gulf of California. *Mar Geodesy* 21(4):245–259
- Rodolfo KS (1969) Bathymetry and marine geology of the Andaman basin and tectonic implications for Southeast Asia. *Geol Soc Am Bull* 80:1203–1230
- Ruff L, Kanamori H (1983) Seismic coupling and uncoupling at subduction zones. *Tectonophysics* 99:99–117
- Sandwell DT, Müller RD, Smith WHF, Garcia E, Francis R (2014) New global marine gravity model from CryoSat-2 and Jason-1 reveals buried tectonic structure. *Science* 346(6205):65–67. <https://doi.org/10.1126/science.1258213>
- Saylor JE, DeCelles P, Gehrels G, Murphy M, Zhang R, Kapp PA (2010) Basin formation in the high Himalaya by arc-parallel extension and tectonic damming: Zhada basin, southwestern Tibet. *Tectonics* 29:TC1004
- Schellart WP (2008) Subduction zone trench migration: slab driven or overriding-plate-driven? *Phys Earth Planet Inter* 170:73–88
- Scholz CH, Campos J (1995) On the mechanism of seismic decoupling and back-arc spreading at subduction zones. *J Geophys Res* 100:22103–22115
- Scotese CR, Gahagan LM, Larson RL (1988) Plate tectonic reconstructions of the Cretaceous and Cenozoic ocean basins. *Tectonophysics* 155:27–48
- Sevilgen V, Stein RS, Pollitz FF (2012) Stress imparted by the great 2004 Sumatra quake shut down transforms and activated rifts up to 400 km away in the Andaman Sea. *Proc Natl Acad Sci U S A* 109:15152–15156
- Shamim Sk, Khan PK, Mohanty SP (2019) Stress reconstruction and lithosphere dynamics along the Sumatra subduction margin. *J Asian Earth Sci* 170:174–187
- Singh SC, Moeremans R (2017) Anatomy of the Andaman–Nicobar subduction system from seismic reflection data. *Geol Soc Lond Mem* 47:193–204
- Singh SC, Carton H, Tapponnier P, Hananto ND, Chauhan APS, Hartoyo D, Bayly M, Moeljopranoto S, Bunting T, Christie P, Lubis H, Martin J (2008) Seismic evidence for broken oceanic crust in the 2004 Sumatra earthquake epicentral region. *Nat Geosci* 1:777–781
- Singh SC, Chauhan APS, Calvert AJ, Hananto ND, Ghosal D, Rai A, Carton H (2012) Seismic evidence of bending and unbending of subducting oceanic crust and the presence of mantle megathrust in the 2004 Great earthquake rupture zone. *Earth Planet Sci Lett* 321–322:166–176
- Singh SC, Moeremans R, McArdle J, Johansen K (2013) Seismic images of the sliver strike-slip fault and back thrust in the Andaman–Nicobar region. *J Geophys Res* 118:5208–5224
- Smith WHF, Sandwell DT (1997) Global seafloor topography from satellite altimetry and ship depth soundings. *Science* 277:1957–1962
- Socquet A, Vigny C, Chamot-Rooke N, Simons W, Rangin C, Ambrosius B (2006) India and Sunda plates motion and deformation along their boundary in Myanmar determined by GPS. *J Geophys Res* 111:B05406
- Song TRA, Simons M (2003) Large trench-parallel gravity variations predict seismogenic behavior in subduction zones. *Science* 301:630–633
- Spector A, Grant FS (1970) Statistical models for interpreting aeromagnetic data. *Geophysics* 35(2):293–302
- Stein S, Okal EA (2007) Ultra-long period seismic study of the December 2004 Indian Ocean earthquake and implications for regional tectonics and the subduction process. *Bull Seismol Soc Am* 97:S279–S295
- Studinger M, Miller H (1999) Crustal structure of the Filchner–Ronne Shelf and Coats Land, Antarctica from gravity and magnetic data: implications for the breakup of Gondwana. *J Geophys Res* 104(B9):20379–20394

- Studinger M, Kurinin RG, Aleshkova N, Miller H (1997) Power spectra analysis of gravity data from the Weddell Sea embayment and adjacent areas. *Terra Antarct* 4(1):23–26
- Subarya C, Mohamed C, Prawirodirdjo L, Avouac J-P, Bock Y, Sieh K, Meltzner AJ, Natawidjaja DH, McCaffrey R (2006) Plate-boundary deformation associated with the great Sumatra–Andaman earthquake. *Nature* 440:46–51
- Subrahmanyam C, Gireesh R, Shyam C, Kamesh Raju KA, Gopala Rao D (2008) Geophysical characteristics of the Ninetyeast Ridge—Andaman Island arc/trench convergent zone. *Earth Planet Sci Lett* 266:29–45
- Tapponnier P, Peltzer G, Armijo R (1986) On the mechanics of the collision between India and Asia. In: Coward MP, Ries AC (eds) *Collision tectonics*. Geological Society of London Special Publication 19:115–157
- Talwani M, Heirtzler JR (1964) Computation of magnetic anomalies caused by two dimensional structures of arbitrary shape. *Computers in the mineral industries, part 452 1*: Stanford University publications. *Geol Sci* 9:464–480
- Talwani M, Lamar WJ, Landisman M (1959) Rapid gravity computations for two-dimensional bodies with application to the Mendocino submarine fracture zone. *J Geophys Res* 64:49–59
- Tiwari VM, Diament M, Singh SC (2003) Analysis of satellite gravity and bathymetry data over Ninety-east Ridge: variation in the compensation mechanism and implication for emplacement process. *J Geophys Res* 108:0148–0227
- Treitel S, Clement WG, Kaul RK (1971) The spectral determination of depths of buried magnetic basement rocks. *Geophys J Roy Astron Soc* 24:415–428
- Tselentis G, Stavrakakis G, Makropoulos K, Latousakis J, Drakopoulos J (1988) Seismic moments of earthquakes at the western Hellenic arc and their application to the seismic hazard of the area. *Tectonophysics* 148:73–82
- Turcotte DL, Schubert G (1982) *Geodynamics applications of continuum physics to geological problems*. Wiley, New York
- Van Keken PE (2003) The structure and dynamics of the mantle wedge. *Earth Planet Sci Lett* 215:323–338
- Weissel JK, Anderson RN, Geller CA (1980) Deformation of the Indo-Australian plate. *Nature* 287:284–291
- Wells RE, Blakely RJ, Sugiyama Y, Scholl DW, Dinterman PA (2003) Basin-centered asperities in great subduction zone earthquakes: a link between slip, subsidence, and subduction erosion? *J Geophys Res* 108:2507. <https://doi.org/10.1029/2002JB002072>
- Wieczorek MA (2007) Gravity and topography of the terrestrial planets. In: *Treatise on Geophysics* Elsevier-Pergamon, Oxford, United Kingdom 10:165–206

Publisher's Note Springer Nature remains neutral with regard to jurisdictional claims in published maps and institutional affiliations.

Authors and Affiliations

Sk. Shamim¹ · Prosanta Kumar Khan¹  · Sarada P. Mohanty² · Manoranjan Mohanty³

✉ Prosanta Kumar Khan
khanprosanta1966@iitism.ac.in

¹ Department of Applied Geophysics, Indian Institute of Technology (Indian School of Mines), Dhanbad 826004, India

² Department of Applied Geology, Indian Institute of Technology (Indian School of Mines), Dhanbad 826004, India

³ Department of Science and Technology, Government of India, New Delhi 110016, India